Plasma Processes and Polymers

PLASMA PROCESSES AND POLYMERS

RESEARCH ARTICLE OPEN ACCESS

Nonthermal Plasma Regeneration of Coke-Deactivated Catalysts Used for Plasma-Catalytic VOC Removal

Jana Kšanová[1] | Richard Cimerman[1] | Oleksandr Galmiz[1,2] | Peter Švec[3] | Karol Hensel[1]

[1]Division of Environmental Physics, Faculty of Mathematics, Physics and Informatics, Comenius University, Bratislava, Slovakia | [2]Department of Plasma Physics and Technology, CEPLANT—R&D Centre for Plasma and Nanotechnology Surface Modifications, Faculty of Science, Masaryk University, Brno, Czech Republic | [3]Institute of Physics, Slovak Academy of Sciences, Bratislava, Slovakia

Correspondence: Richard Cimerman (richard.cimerman@fmph.uniba.sk)

Received: 22 October 2025 | **Revised:** 12 March 2026 | **Accepted:** 25 March 2026

Funding: Slovak Research and Development Agency, Grant/Award Number: APVV-20-0566; EU NextGenerationEU through the Recovery and Resilience Plan for Slovakia, Grant/Award Number: 09I03-03-V04-00092

Keywords: catalysis | catalyst deactivation | dielectric barrier discharges (DBD) | plasma regeneration | toluene removal

ABSTRACT

The research was focused on oxygen nonthermal plasma regeneration of coke-deactivated catalysts used for plasma-catalytic toluene removal from air. The nonthermal plasma was generated in a packed-bed dielectric barrier discharge reactor at atmospheric pressure using pellet-shaped catalysts (TiO_2, γ-Al_2O_3, Pt/γ-Al_2O_3, Pd/γ-Al_2O_3). Gaseous products of experiments were continuously analyzed by infrared spectroscopy. Plasma regeneration was compared with ozone and thermal regeneration. The results indicated that the plasma regeneration exhibited the highest coke removal efficiency; however, the regeneration was spatially non-uniform, as confirmed by SEM and TGA. The effect of ozone and heat (100°C) was negligible. GC–MS analysis revealed that coke composed of long-chain alkanes and oxygen- or nitrogen-substituted aromatics was significantly reduced after plasma regeneration, unlike other regeneration techniques.

1 | Introduction

As it is well-known, plasma catalysis, i.e., a combination of nonthermal plasma (NTP) with conventional catalysis, can utilize both a high plasma reactivity along with a high catalyst selectivity [1]. Therefore, the application of plasma catalysis may lead to enhanced process efficiency and lower energy consumption when compared to individual NTP or catalytic processes [2]. In recent years, the plasma catalysis has shown promising results in many applications including gas [3, 4] and water [5, 6] pollution control, carbon dioxide conversion [7, 8], fuel reforming [9, 10], etc.

However, plasma catalysis does not always yield optimal results, as its effectiveness can depend strongly on specific reaction conditions and system configurations. More specifically, when the application of plasma catalysis is not fully optimized, the process efficiency and product selectivity can still be low. For example, the application of plasma catalysis for dry reforming of methane CH_4 may result in the formation of black carbon (e.g., soot or coke) as an undesired by-product [11, 12]. Another example is the application of plasma catalysis for the removal of volatile organic compounds (VOCs). In addition to desired products (e.g., carbon dioxide CO_2, water vapor H_2O), the formation of many undesired by-products (e.g., ozone O_3, nitrogen oxides NOx, carbon monoxide CO, complex organic compounds) can also be present [13, 14]. The complex organic by-products (such as benzaldehyde, benzene, formic acid, benzyl alcohol, nitrophenols) usually adsorb or condense on the inner walls of the experimental system as well as on the surface of the catalyst and form solid coke (i.e., carbon-containing) deposits [15, 16]. As a result, the catalyst is gradually deactivated, and its activity, selectivity, and overall process efficiency may be significantly reduced.

In general, catalyst deactivation, i.e., the loss of catalytic activity or selectivity over time, is one of the major and inevitable concerns not only in plasma catalysis but also in conventional catalysis [17]. There are several causes of catalyst deactivation: catalyst poisoning, fouling, attrition, crushing, and thermal degradation. After a decline in catalyst activity/selectivity, the catalyst can be discarded, recycled, used for another application or regenerated (restored) [18]. From the economic and environmental point of view, the last option is the most appropriate. The most frequent type of catalyst deactivation is the fouling of the catalyst surface by coke deposits [18]. In this case, the conventional regeneration methods include gasification, chemical washing, hydrogenation, mechanical, and thermal catalyst treatment [19]. The catalyst gasification and hydrogenation is the removal of coke deposits by chemical reactions (oxidation, reduction) when a proper reactant (O_2, H_2, H_2O, or CO_2) is added to the gas mixture. Gasification in the O_2 atmosphere and, thus, oxidation of the coke deposits is usually a preferred route, however, the exothermicity of the reaction can result in catalyst overheating, leading to loss of its surface area and unwanted chemical reactions [19]. The chemical washing with chlorobenzene or liquified propane as solvents can also be used. This method can remove deposits from the catalyst, but may cause unwanted chemical changes on the catalyst surface, so it is not generally applicable to all types of deposits. Mechanical regeneration like ultrasonic cleaning can also cause irreversible mechanical damage to the catalyst. Finally, a thermal regeneration, although popular due to its simplicity and effectiveness, has high energy costs as it requires high operating temperatures (up to 900°C) [18, 20]. Besides, the catalyst overheating can often lead to its sintering, i.e., a loss of surface area or undesired surface chemical reactions [18]. For these reasons, there has been an increasing interest in inexpensive, economically, and energetically feasible methods of catalyst regeneration that would preserve the material of the catalyst with minimal changes to its surface properties.

In addition to the applications of plasma catalysis mentioned above, the combination of plasma with catalysis may also be applied for the regeneration of the catalysts. As is widely known, the NTP can create a highly reactive environment comprising of many reactive species including ions, metastables, excited species etc. [21]. These species may interact with the surface of the deactivated catalysts and initiate chemical reactions leading to catalyst regeneration. In the case of the fouled catalysts deactivated by undesired coke deposits, the principle of plasma regeneration lies in oxidation of deposits with simultaneous recovery of the physicochemical properties of the catalyst. Under NTP treatment in O_2 atmosphere, oxygen reactive species (e.g., ·O, O^-, O_2^+, O_2^-, O_3) along with other radicals (e.g., ·OH, ·H, $\cdot HO_2$ generated under humid gas conditions) are considered to play vital roles in plasma-initiated oxidation of coke deposits [22, 23]. As a result, the plasma regeneration of coke-deactivated catalysts leads to the formation of gaseous oxidation products (e.g., CO, CO_2, H_2O) [23, 24]. Additionally, the interaction between the NTP and the catalyst has been reported to cause minimal damage to the original catalyst structure [25], and it may even increase the average pore size and improve the overall pore structure of the catalyst [26]. Besides, the NTP can produce the reactive species even at ambient conditions, i.e., at atmospheric pressure and room temperature [27, 28]. This represents the greatest advantage in contrast to other catalyst regeneration techniques, as it allows for a substantial decrease in energy requirements.

Several authors have investigated the use of NTP generated by atmospheric-pressure discharges for the regeneration of deactivated catalysts, as reviewed by Pinard et al. [23] or Lee et al. [29]. The cylindrical (tubular) or pin-to-plate dielectric barrier discharge (DBD), and glow discharge have been usually used [23]. DBD in a tubular geometry is very popular arrangement as it allows for the filling of the reactor with solid catalysts in the form of small spherical or cylindrical pellets. Hence, the so-called packed-bed DBD has been the most frequently investigated for catalyst regeneration [30–32].

The first group of studies focused on the regeneration of catalysts previously deactivated by adsorbed VOCs. Hossian et al. [30] and Veerapandian et al. [33] both studied the regeneration of catalysts deactivated by adsorbed toluene using NTP generated by a packed-bed DBD reactor in dry air. Hossian et al. [30] showed that the zeolite with adsorbed toluene was effectively regenerated during the plasma regeneration. Veerapandian et al. [33] reported that the catalytic activity and CO_2 selectivity of plasma-regenerated hopcalite slightly increased, in contrast to fresh hopcalite, although the specific surface area was reduced. The observed effect was explained by the higher ratio of oxygen adsorbed at the surface to oxygen bound in the hopcalite after the plasma regeneration. Mok et al. [34] investigated the regeneration of γ-Al_2O_3 previously deactivated by adsorbed toluene using a packed-bed DBD reactor in oxygen. They demonstrated that the time required to oxidize the adsorbed toluene decreased with the increasing discharge power. Wang et al. [35] investigated the regeneration of various catalysts previously deactivated by adsorbed toluene using a two-stage DC plasma upstream configuration at a fixed relative humidity of 40% and room temperature. They noted that intermittent use of adsorption and plasma regeneration can reduce energy consumption and by-products. Kuroki et al. [36] studied the regeneration of honeycomb zeolite deactivated by adsorbed toluene by using pulsed NTP. They studied the effect of gas flow rate on toluene desorption and catalyst regeneration efficiency and found their increase when a gas flow was stopped for a certain time. The above-mentioned studies on the regeneration of catalysts deactivated by adsorbed VOCs indicates that upon application of NTP, it is possible to achieve not only efficient VOC desorption (> 50%), but also high VOC removal efficiency (typically 70%–100%).

In addition to the regeneration of catalysts deactivated by adsorbed VOCs, the second group of studies demonstrated the plasma regeneration of coke-deactivated catalysts. For instance, Jia et al. [37] and Pinard et al. [23] investigated regeneration of coked zeolites deactivated after pyrolysis of oak using a DBD reactor with a pin-to-plate geometry at room temperature. Both groups of authors noted that the efficiency of regeneration is directly related to the number of active species in the gas phase. Among the regeneration products, CO, CO_2, light organic compounds and carboxylic acids were observed [37]. Di et al. [32] studied the plasma-catalytic removal of o-xylene in air using a DBD reactor filled with Pt-, Pd- and Au/Co_3O_4 catalysts with their subsequent plasma regeneration. The coke-deactivated catalysts resulting from o-xylene removal were investigated with or without a simultaneous flow of o-xylene. In

both cases, they found that oxidation of coke on the catalyst surface to COx is faster at a higher temperature (80°C). Srour et al. [38] compared the regeneration efficiency of aged industrial hydrodesulfurization catalyst $CoMoP/Al_2O_3$ by thermal and plasma oxidations. It was observed that using the NTP, a total removal of coke was obtained at a lower temperature (250°C) compared to conventional thermal regeneration (500°C). Al-Jalal et al. [39] used low-pressure glow discharge to regenerate coked-deactivated Pt/Al_2O_3 in $He-O_2$ or $Ar-O_2$ mixtures and performed detailed optical emission spectroscopy measurements. They demonstrated that ·O radicals in the glow discharge dominate the process of coke oxidation, yielding to emission of ·H, CO, CO_2, and other carbon complexes in the emission spectra. The review of recent studies suggests that the NTP regeneration of coke-deactivated catalysts is considerably more challenging than the desorption of adsorbed VOCs from the catalysts, particularly under low-temperature conditions. The number of available results and knowledge remains still limited even more in a specific case of catalysts deactivated by flue-gas cleaning processes. This evident knowledge gap highlights the need for systematic studies. Further research is, therefore, essential to clarify the mechanisms and optimize regeneration strategies under specific NTP operating conditions.

In this work, the plasma regeneration of various coke-deactivated catalysts was investigated. Firstly, deactivation of the catalysts was performed by removal of the model target VOC compound (toluene) from the air using the plasma-catalytic packed-bed DBD reactor. The toluene removal resulted in the formation of many products, some of which gradually accumulated on the catalyst surface and created solid coke deposits. Secondly, the coke-deactivated catalyst was regenerated using an identical packed-bed DBD reactor in an O_2 atmosphere. The experiments were carried out using several materials with distinctly different physical and chemical characteristics (dielectric constants, redox properties, etc.), including TiO_2, γ-Al_2O_3, Pt/γ-Al_2O_3, and Pd/γ-Al_2O_3. Out of them, γ-Al_2O_3 is usually considered to have very limited catalytic properties for toluene removal, and it is often used as a support (base) material for supported catalysts [40]. However, certain studies revealed it may have specific catalytic properties for other applications [41]. For these reasons and for the sake of simplicity, we will further refer to all materials tested as catalysts. TiO_2 was selected owing to its photocatalytic activity [42], Pt– and Pd/γ-Al_2O_3 due to their well-known oxidative properties [43], and γ-Al_2O_3 as reference support with reliable structural properties [44]. Such broad comparison of various catalysts is usually absent in existing plasma regeneration studies, strengthening the novelty of this research approach. The gaseous products of the toluene removal, as well as the gaseous products of the regeneration, were monitored using Fourier-transform infrared (FTIR) absorption spectroscopy. In addition, to directly address the outlined research gap, a comparison of plasma regeneration with alternative techniques (ozone and thermal regeneration) was also performed. It was essential for determining whether catalyst regeneration results from plasma or merely from secondary effects such as ozone oxidation or heat exposure. Finally, chemical identification of solid coke deposits was performed by gas chromatography-mass spectroscopy (GC-MS) analysis and the surface of the catalysts was analyzed by scanning electron microscopy (SEM) and thermogravimetric analysis (TGA).

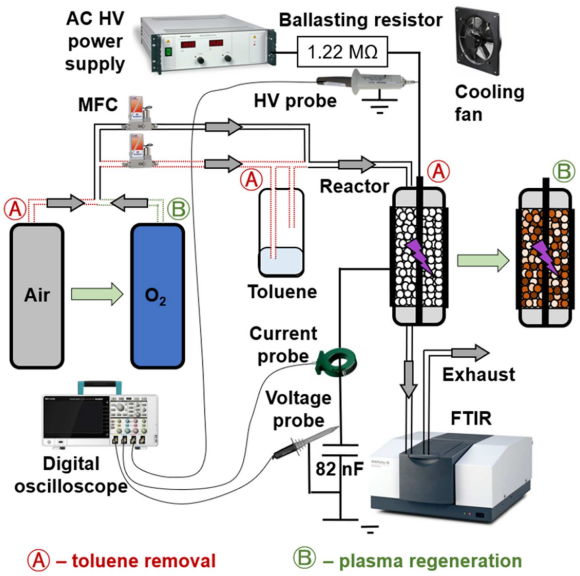

FIGURE 1 | Experimental setup for toluene removal Ⓐ and plasma regeneration Ⓑ.

2 | Experimental Setup and Methods

The experimental setup is depicted in Figure 1. The experiment consisted of two steps. Firstly, the experimental setup was employed for the toluene removal by plasma catalysis (marked as Ⓐ in Figure 1). Secondly, the coke-deactivated catalyst from the previous step was regenerated by the plasma (Ⓑ). In both steps of the experiment, the NTP was generated by packed-bed DBD reactors of cylindrical geometry. The reactors consisted of a quartz glass tube with an inner diameter of 14 mm and a thickness of 2 mm that served as a dielectric barrier. The length of the tube varied in different experiments (10 or 4.5 cm). An aluminum tape was wrapped around the tube serving as an external grounded electrode. A brass rod with a diameter of 6 mm placed in the axis of the tube was used as the internal electrode and was connected to an AC high voltage (HV) power supply. A gas gap between the internal electrode and the quartz glass tube was packed with pellets of various compositions with spherical (TiO_2, γ-Al_2O_3, Pt/γ-Al_2O_3) or cylindrical (Pd/γ-Al_2O_3) shape with a diameter of 2–4 mm. The tube was closed on both ends with plugs allowing a gas inlet and outlet. The AC HV power supply consisted of a function generator (FeelElec FY-6900), a signal amplifier (RH Sound SK11500) and an HV transformer. The HV power supply was connected to the internal electrode of the reactor through a ballasting resistor (1.22 MΩ), which was cooled by a fan. Upon application of HV, a DBD was generated inside the reactor in the gas gaps among the pellets. The waveforms of the applied voltage were measured by a HV probe (Tektronix P6015A) and the discharge current by a current probe (Pearson Electronics 2877), both connected to a digital oscilloscope (Tektronix TBS2104). The discharge power was evaluated by the method of Lissajous (charge-voltage) figures, which provides an accurate evaluation of the real power of DBD reactors. The applied voltage was measured using a HV probe (Tektronix 2220), and the transferred charge was obtained from the voltage drop across a reference capacitor (82 nF). For each operating point, the evaluated charge q was plotted against the applied voltage V to

form a Lissajous figure, and the enclosed area was integrated to obtain the discharge power P:

$$P = f \times \oint V \times \mathrm{d}q, \tag{1}$$

where f is the applied voltage frequency (1 kHz) [45–47]. The gases (synthetic air or oxygen) were supplied from pressure cylinders, and their flow rates were controlled by mass flow controllers (MFC) (Bronkhorst El-Flow Prestige FG-201CV). The gas analysis was performed by FTIR spectrometer (Shimadzu IR-Affinity 1S, Shimadzu IRSpirit) using a gas cell with an optical path length of 10 cm equipped with KRS-5 windows.

2.1 | Toluene Removal

The first step of the experiment consisted of toluene C_7H_8 removal (marked as Ⓐ in Figure 1). In this case, synthetic air (80% N_2 + 20% O_2) with a purity 5.0 was used as a carrier gas. The air flow was split into two gas lines (marked as Ⓐ in Figure 1), while the total air flow rate was fixed at 0.5 L/min. The air from the first line was enriched with toluene vapors in the bubbler and then mixed with the air from the second line in order to obtain the desired initial toluene concentration (approx. 3200 ppm). The gas mixture was subsequently led into a packed-bed DBD reactor with a length of a quartz glass tube of 10 cm. The amplitude of the applied voltage was adjusted to obtain a fixed discharge power of 6 W (i.e., 720 J/L) regardless of the catalyst used (TiO_2, γ-Al_2O_3, Pt/γ-Al_2O_3, Pd/γ-Al_2O_3). The toluene removal was performed at room temperature with a fixed duration of 3 h.

During the first step of the experiment, toluene was decomposed by NTP into various gaseous and solid products. Toluene along with gaseous products carbon dioxide CO_2, carbon monoxide CO and formic acid HCOOH were determined both qualitatively and quantitatively (in ppm units) based on their previous FTIR calibrations at wavenumbers of 729, 2360, 2169, and 1105 cm^{-1}, respectively. Besides, the production of various solid products was also observed as they gradually adsorbed and accumulated on the surface of the catalysts and reactor walls, creating solid coke deposits.

The performance of the used DBD reactors was evaluated with the help of the following variables: specific energy input (SEI) (i.e., energy density), toluene removal efficiency (TRE), energy cost (EC), carbon balance (CB), and selectivity. They were calculated according to Equations (2) to (6) as follows:

- SEI:

$$\mathrm{SEI\ [J/L]} = \frac{P\ [W] \times 60}{Q\ [\mathrm{L/min}]}, \tag{2}$$

where P and Q represent the input power and total gas flow rate, respectively.

- TRE:

$$\mathrm{TRE\ [\%]} = \left(1 - \frac{c\ \ [\mathrm{ppm}]}{c_0\ [\mathrm{ppm}]}\right) \times\ 100, \tag{3}$$

where c_0 and c represent the input (initial) and output concentrations of toluene, respectively.

- EC:

$$\mathrm{EC\ [kWh/kg]} = \frac{\mathrm{SEI\ [J/L]}\ \times\ 277.\,8}{\mathrm{TRE}\ \times\ c_0\ [\mathrm{mg/m^3}]}, \tag{4}$$

where the factor of 277.8 comes from the conversion of J units to kWh.

- CB:

$$\mathrm{CB\ [\%]} = \frac{c(\mathrm{CO_2})\ [\mathrm{ppm}] + c(\mathrm{CO})\ [\mathrm{ppm}] + c(\mathrm{HCOOH})\ [\mathrm{ppm}]}{n \times \mathrm{TRE} \times c_0\ [\mathrm{ppm}]} \times 100, \tag{5}$$

where $c(CO_2)$, $c(CO)$, and $c(HCOOH)$ are the concentrations of the given gaseous products of toluene removal, n is the number of carbons in the toluene molecule ($n = 7$) and c_0 represents the input (initial) concentration of toluene.

- *Selectivity* (S):

$$\mathrm{S\ [\%]} = \frac{c(\mathrm{X})\ [\mathrm{ppm}]}{n \times \mathrm{TRE} \times c_0\ [\mathrm{ppm}]} \times 100, \tag{6}$$

where c(X) is the concentration of the given gaseous product X of toluene removal.

2.2 | Regeneration of Coke-Deactivated Catalysts

In the second step of the experiment, the coke-deactivated catalysts from the toluene removal experiments were subsequently regenerated to remove solid deposits from their surface to restore their catalytic activity. Various methods of regeneration were used (plasma, thermal, and ozone) with a fixed duration of 2 h. The length of the quartz glass tube of the packed-bed DBD reactor for plasma regeneration, as well as the length of the catalyst bed for thermal and ozone regeneration was 4.5 cm.

2.2.1 | *Plasma Regeneration*

The experimental setup for plasma regeneration (marked as Ⓑ in Figure 1) was almost identical to that for toluene removal. In this case, the packed-bed DBD was filled with a coke-deactivated catalyst from the previous toluene removal experiment, while the oxygen with a purity 2.5 was used as a carrier gas with a flow rate of 0.5 L/min. The plasma regeneration was performed with a fixed discharge power of 3 W (i.e., 360 J/L) regardless of the catalyst used.

2.2.2 | *Ozone Regeneration*

Ozone is known to be a strong oxidizer. During plasma regeneration by packed-bed DBD reactors, O_3 is generated along with other reactive species and radicals. To understand its individual contribution, the ozone regeneration of coke-deactivated catalysts was also investigated. The experimental setup for ozone

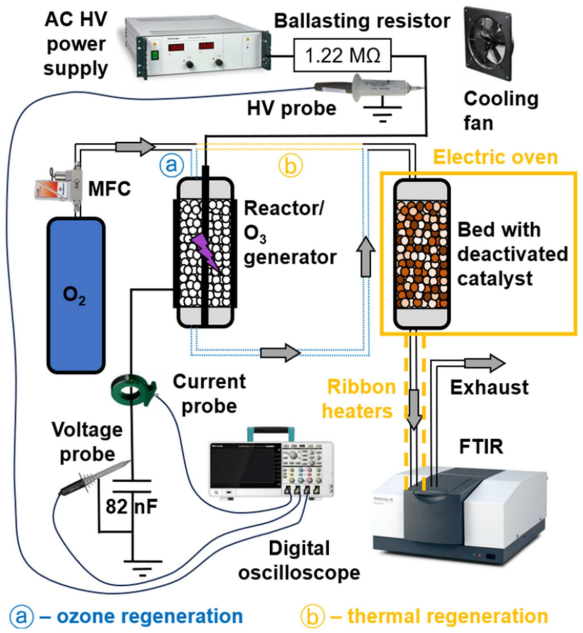

FIGURE 2 | Experimental setup for the ozone ⓐ and thermal regeneration ⓑ.

regeneration is depicted in Figure 2 and marked as ⓐ. As an O_3 generator, the packed-bed DBD reactor filled with TiO_2 pellets was used and fed by oxygen with a flow rate of 0.5 L/min. The gas mixture of oxygen and O_3 was then led into the catalyst bed filled with coke-deactivated catalysts. The initial ozone concentration was approximately 8000 ppm which corresponds to the steady-state ozone concentration produced during plasma regeneration. O_3 was qualitatively and quantitatively determined based on its previous FTIR calibrations at wavenumber of 1055 cm^{-1}.

2.2.3 | *Thermal Regeneration*

During the plasma regeneration, the packed-bed DBD reactors heated up to approx. 70°C at the maximum power. To assess the potential impact of the plasma-generated heat on the catalyst regeneration, thermal regeneration was also conducted. The experimental setup for thermal regeneration is depicted in Figure 2 and marked as ⓑ. Similar to plasma regeneration, oxygen was used as a carrier gas with a flow rate of 0.5 L/min. The gas was then fed into the catalyst bed filled with coke-deactivated catalysts. The electric oven was used to heat the catalyst bed, while ribbon heaters were employed to heat the gas lines and the FTIR gas cell to 100°C, which is slightly above the temperature generated by the discharge.

2.3 | Advanced Analyses

In addition to FTIR gas analysis, several advanced analyses of catalysts and solid deposits were also carried out.

2.3.1 | *SEM Analysis*

The SEM analysis (Tescan MIRA3; Thermo Scientific Apreo2S) was used to characterize the surface morphology of the fresh, deactivated, and regenerated catalysts. Secondary electrons (SEs) were used to obtain micrographs providing information about the surface topography. In the SE micrographs presented in this paper, a magnification of ×2000 and an electron accelerating voltage of 10 kV were applied.

2.3.2 | *GC-MS Analysis*

The GC-MS was used to identify solid coke deposits accumulated on the surface of the catalysts after toluene removal as well as catalyst regeneration experiments. The catalysts were immersed in a closed sample containers with 20 mL of isopropanol to dissolve the coke deposits. Subsequently, after 72 h of extraction at room temperature, the sample containers were opened and placed in a fume hood. Over the next 24 h, approximately 50% of the isopropanol was evaporated to increase the concentration of deposits in the solvent, and the residual solution was used for GC-MS measurements. A GC-MS instrument (Shimadzu GC-2010 & GCMS-QP2010 Plus) equipped with a capillary column (Restek RTX-5MS) was used for analysis. The injector temperature was set to 300°C, the split ratio was 30, and the injection volume of a sample was 8 μL. The initial oven temperature was set to 50°C and held for 5 min. Then, a heating rate of 10°C/min was set with a maximum temperature set to 200°C. The total duration of an analysis for one sample was 20 min. Identification of the molecules in the mass-to-charge ratio range of 40–500 was performed with GC-MS software. Measurements using pure isopropanol served as a reference to exclude solvent signals or other artifacts [48].

2.3.3 | *TGA*

The TGA (Perkin Elmer TGA7) provided accurate tracking of the weight change of the catalysts under controlled and gradual temperature increase in a dynamic inert argon atmosphere (60 mL/min). With controlled temperature increase, a gradual desorption of solid coke deposits from the surface of the catalyst occurred. Weight change of the catalysts allowed for a determination of the relative amount of volatile deposits on both deactivated and regenerated catalysts. The starting temperature was set to 40°C and the heating rate to 10°C/min until a maximum temperature (800°C) was reached. The sample amount was held in the range of 40–60 mg, for all the studied catalysts.

3 | Results and Discussion

3.1 | Voltage and Current Waveforms

Figure 3a–d presents the voltage and current waveforms of packed-bed DBD reactors filled with TiO_2 and Pt/γ-Al_2O_3 catalysts. Figure 3a,b shows typical waveforms of the plasma reactors used for toluene removal in synthetic air. The amplitude of the applied voltage was adjusted to obtain a fixed discharge power of 6 W, regardless of the catalyst used, and ranged from 12 to 13 kV. On the other hand, Figure 3c,d represents typical waveforms of the plasma reactors used for plasma regeneration in oxygen. In this case, the discharge power was fixed to 3 W, and the amplitude of the applied voltage was also adjusted accordingly (from 14 to 16 kV). It is evident that the current waveforms of reactors in air generally exhibited more

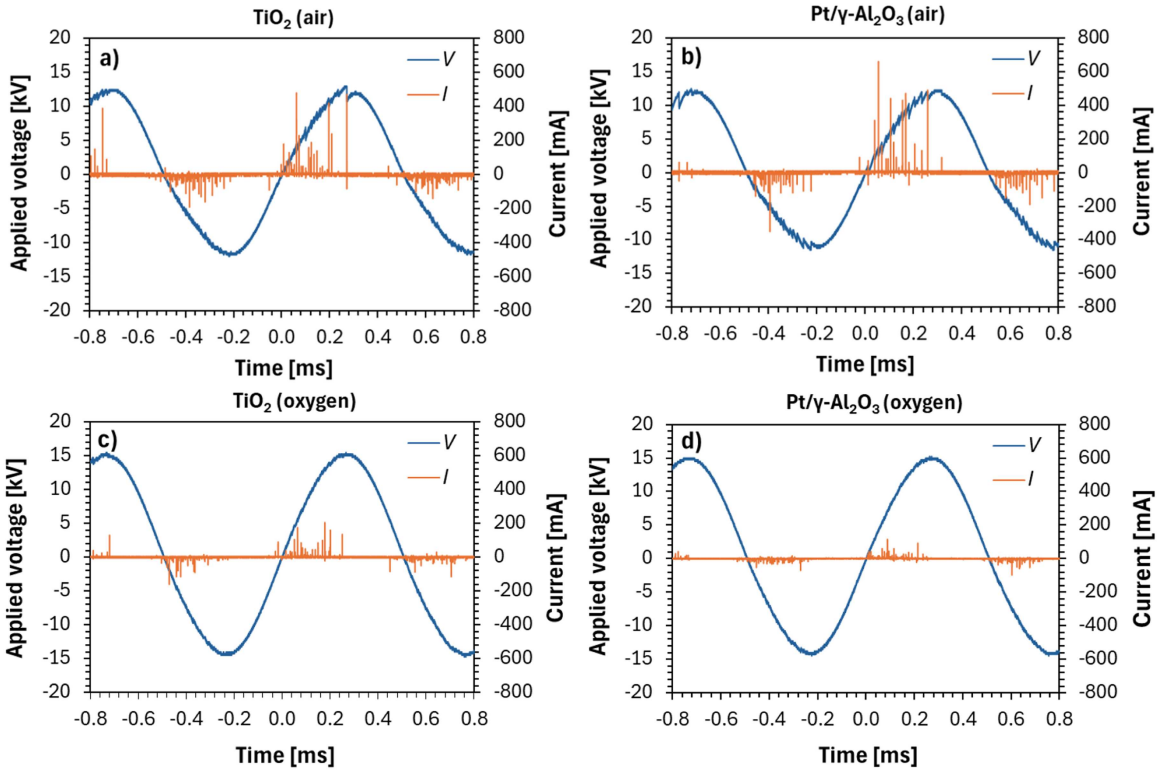

FIGURE 3 | (a–d): Voltage V and current I waveforms of packed-bed DBD reactors filled with (a) TiO_2 and (b) Pt/γ-Al_2O_3 in synthetic air (6 W); (c) TiO_2 and (d) Pt/γ-Al_2O_3 in O_2 (3 W).

current pulses with higher amplitudes than in oxygen, as a result of the electronegative character of oxygen [49].

In general, behavior of packed-bed DBDs is strongly influenced by the dielectric constant (ε_r) of the pellets, which plays a key role in determining the discharge mode. Higher-ε_r materials concentrate the electric field at the contact points between the pellets, promoting formation of intense and localized microdischarges (i.e., localized microdischarge mode). In contrast, lower-ε_r materials result in a more diffuse field distribution, formation of surface discharges and a smaller degree of microdischarges localization (i.e., surface discharge mode). In case of medium-ε_r materials, the discharge may exhibit characteristics of both modes (i.e., mixed discharge mode) [46, 50, 51]. In addition to ε_r, the local electric field enhancement and, consequently, the discharge mode can be further influenced by other factors, such as pellet porosity [52] and metal loading of the catalyst [53]. The dielectric constants of the materials used in this study are therefore considered as effective permittivity values reported in the literature for porous catalyst pellets under DBD conditions ($\varepsilon_r \approx 7$–11 for γ-Al_2O_3, Pt/γ-Al_2O_3 and Pd/γ-Al_2O_3, and $\varepsilon_r \approx 20$–100 for TiO_2) [50, 54, 55]. These effective permittivities collectively account for the combined influence of material properties governing the discharge mode [56]. Based on this, surface discharge or mixed discharge modes may be expected under our experimental conditions. This interpretation is consistent with the visual observations of the discharges as well as recorded current waveforms and Lissajous figures (not shown). The current waveforms are characterized by the presence of numerous current pulses with low to medium amplitudes, depending on the type of catalyst and carrier gas used. The consistency between the recorded current waveforms and the shape of corresponding Lissajous figures further indicates the absence of intense microdischarges or arcing and supports the reliability of the power determination, with the reported power values directly reflecting the energy deposited into the reactors.

3.2 | Toluene Removal

3.2.1 | *Toluene Removal Efficiency*

Figure 4a shows the TRE obtained with different catalysts. The TREs were found in the order as follows: TiO_2 (57%) < γ-Al_2O_3 (65%) < Pt/γ-Al_2O_3 (74%) < Pd/γ-Al_2O_3 (76%). The highest and similar TREs were reached by using Pd/γ-Al_2O_3 and Pt/γ-Al_2O_3. Both catalysts are generally characterized by high catalytic oxidation activity [57], so these results were expected. The TRE obtained with γ-Al_2O_3 was surprisingly found to be higher than with TiO_2. TiO_2 is a well-known photocatalyst that requires UV radiation (< 400 nm) of sufficient intensity for its activation [42]. In the case of plasma catalysis, it can be additionally activated by the impact of electrons, ions, or metastables carrying sufficient energy [58, 59]. However, few studies reported that the energy of electrons, ions, and especially the intensity of UV radiation in the NTP may not be sufficient to activate the photocatalyst in plasma catalysis [60]. Therefore, the photocatalytic activity of TiO_2 in plasma catalysis is questionable, especially under conditions of relatively low discharge energy densities, as we worked with. On the other hand, a relatively high TRE reached with γ-Al_2O_3 may lie in the fact that catalysts of different properties may affect the generated plasma in various ways, which in turn may influence TRE itself. It is well-

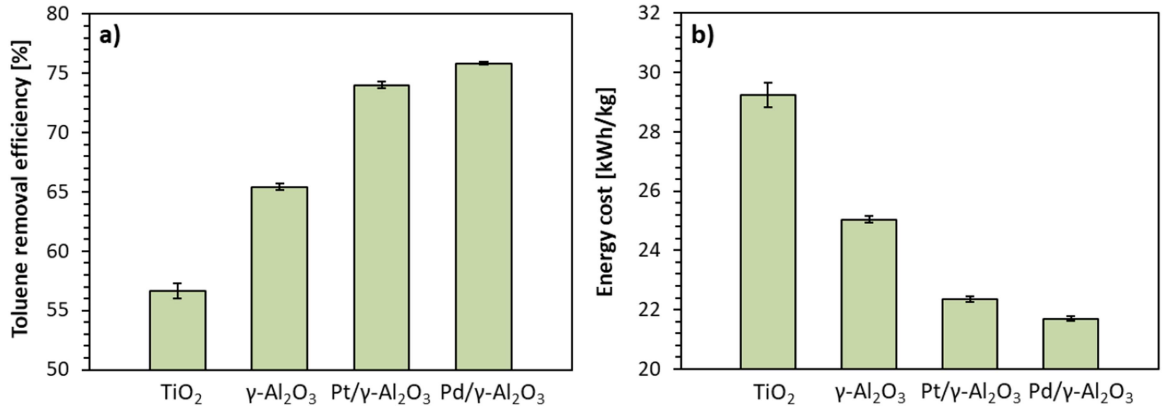

FIGURE 4 | (a, b): Toluene removal efficiency (a) and associated energy cost (b) obtained with different catalysts (6 W).

known that the dielectric constant of the catalysts plays a crucial role in the discharge mode of the packed-bed DBD reactor [51, 61]. Since γ-Al_2O_3 has a lower dielectric constant (~7–11) than TiO_2 (~20–100), the discharges preferentially propagate over its surface without the formation of intense and localized microdischarges typical for materials with medium (such as TiO_2) and high dielectric constants. Additionally, γ-Al_2O_3 we used has a larger specific surface area (~300 m^2/g) than TiO_2 (~70 m^2/g) [13], which may substantially affect the adsorption capacity for toluene as well as its decomposition intermediates. Therefore, we assume a different adsorption capacity combined with dominant surface discharges can potentially explain the higher TRE achieved with γ-Al_2O_3 compared to TiO_2. The similar result, i.e., higher TRE with γ-Al_2O_3 than with TiO_2, was also reported by Iervolino et al. [62]. They also attributed the observed effect to the greater adsorption capacity of γ-Al_2O_3.

In addition to TRE, ECs obtained with all catalysts were also evaluated and reached the order as follows: TiO_2 (29.2 kWh/kg) > γ-Al_2O_3 (25.0 kWh/kg) > Pt/γ-Al_2O_3 (22.4 kWh/kg) > Pd/γ-Al_2O_3 (21.7 kWh/kg) (Figure 4b).

The toluene removal by plasma catalysis has been studied by many authors, as toluene is very often used as a model target VOC compound. The results obtained are very well documented in review studies by Vandenbroucke et al. [63], Xiao et al. [64], and Veerapandian et al. [65].

Among studied catalysts, Pt/γ-Al_2O_3 and Pd/γ-Al_2O_3 were used for toluene removal from dry air by Harling et al. [66]. They achieved TRE over 95%; however, this was obtained at a higher gas temperature (300°C), substantially lower toluene input concentration (200 ppm) and SEI (60 J/L) compared to our system. High activity of Pt/γ-Al_2O_3 was also reported by Kim et al. [67] with TRE of 98%; however, again at lower toluene input concentration (110 ppm) and lower SEI (210 J/L). Low input toluene concentration of 215 and 220 ppm was also used by Holzer et al. [68] and Song et al. [69] in dry and humid air, respectively. They both used γ-Al_2O_3 and obtained TRE of approx. 53% and 65% at ambient temperature; however, with substantially different SEI of approx. 2400 and 110 J/L, respectively. TiO_2 catalyst was tested in combination with $BaTiO_3$ by Liang et al. [70, 71]. They reported TRE of approx. 65% at SEI of 340 J/L at toluene input concentration of 184 ppm. Combination of TiO_2 with $BaTiO_3$ was also found to be beneficial as reported by Wang et al. [72]. While TiO_2 acted as a photocatalyst, $BaTiO_3$ was utilized to enhance the electric field in the plasma reactor, what significantly enhanced the toluene removal. Finally, TiO_2 in combination with γ-Al_2O_3 was investigated by Zhu et al. [73] with TRE of approx. 88% at 700 J/L and toluene input concentration of 263 ppm.

As reported, most of the authors worked with toluene input concentrations lower than 200 ppm, i.e., one order of magnitude lower than we worked with (3200 ppm). Only a few authors have worked with higher toluene concentrations. For example, both Kang et al. [74] and Chang et al. [75] removed toluene using the packed-bed DBD reactor filled with TiO_2 at toluene input concentration of 1000 and 1100 ppm, respectively [74, 75]. Kang et al. [74] achieved the TRE of 70% at a SEI of 360 J/L, while Chang et al. [75] reported a maximum TRE of 78% at SEI of 1000 J/L. Relatively high input toluene concentration represents conditions that are usually less favorable to achieve high removal efficiencies [76]. It should be noted here that our research did not focus on maximizing and optimizing the TRE and EC values, but basically only on the fouling of the catalysts during the process of toluene removal from the air for their subsequent regeneration. Our results on toluene removal serve here mainly as a reference and are presented along with results achieved by other groups for a brief comparison. In this sense, the results obtained are reasonable and provide a good starting point for future applications where high concentrations of toluene (or other VOCs) are unavoidably present.

3.2.2 | *Toluene Removal Products*

The FTIR spectra in Figure 5 show both gaseous and solid products of the toluene removal using Pt/γ-Al_2O_3 catalyst. The solid products were found as coke deposits accumulated on the surface of catalysts, reactor walls, inside the gas lines, as well as on the windows of the FTIR gas cell. The spectrum of solid products belongs to deposits accumulated on the windows of the gas cell during the experiment. It was recorded after the discharge was switched off and the gas cell was flushed with dry air to remove all gaseous products. On the other hand, the spectrum of gaseous products was obtained indirectly. Firstly, a combined spectrum of gaseous and solid products was obtained after 120 min, before the discharge was switched off. Subsequently, the spectrum of solid products was subtracted from the combined spectrum to obtain a spectrum of only gaseous products.

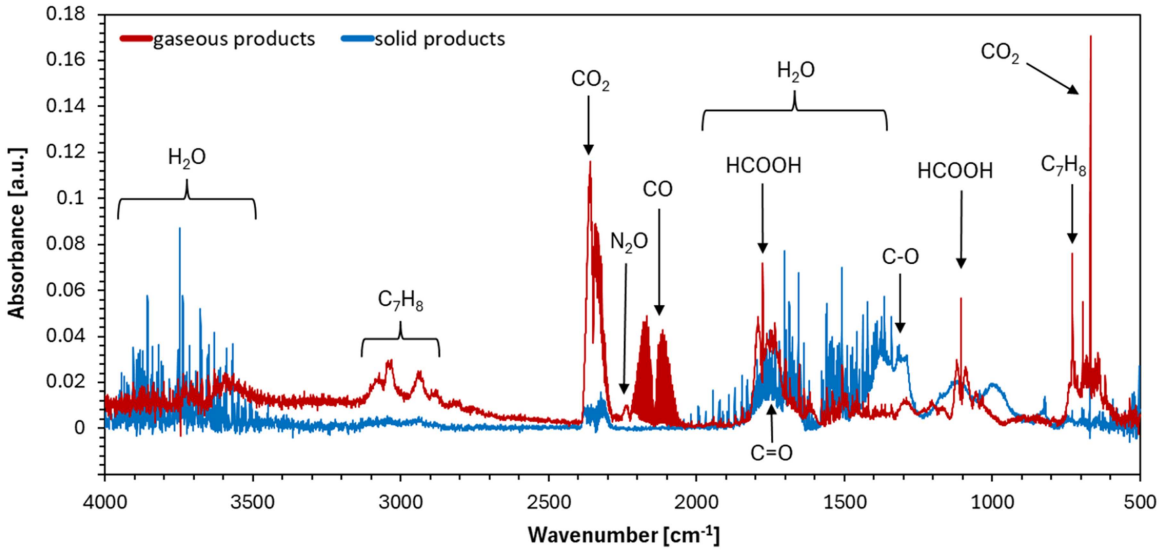

FIGURE 5 | FTIR spectra of gaseous and solid products of toluene removal using Pt/γ-Al_2O_3.

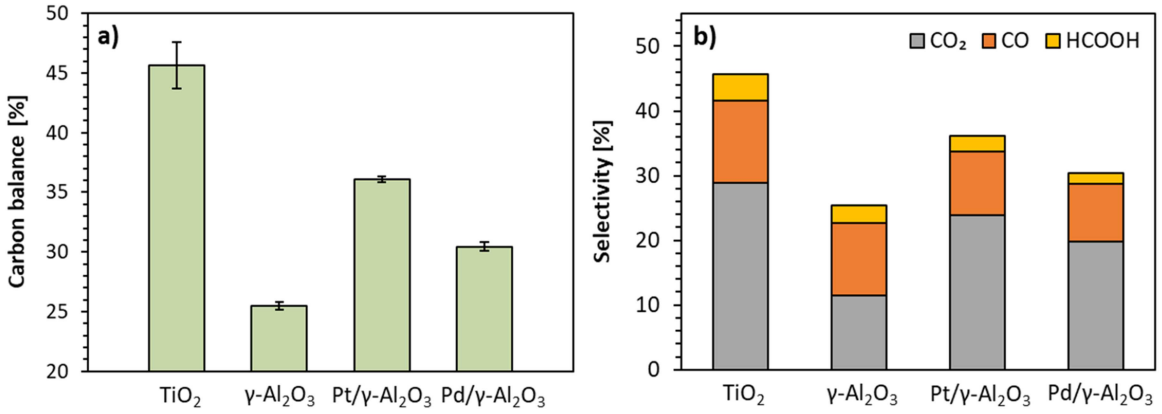

FIGURE 6 | (a, b): Carbon balance (a) and selectivity of CO_2, CO, and HCOOH (b) for toluene removal obtained with different catalysts.

Among the gaseous products (red spectrum in Figure 5), CO_2, CO, and HCOOH were observed. These products are typical for toluene oxidation in air. Nitrous oxide N_2O was also formed in small quantities as a result of discharge-initiated reactions of N_2 and O_2. In the spectra, absorption bands of water vapors H_2O are also present. These bands may arise from the formation of H_2O as a product of toluene oxidation or from the desorption of moisture from the catalysts. On the other hand, the identification of solid products is challenging due to relatively low, broad, and overlapping absorption bands (blue spectrum in Figure 5 from 800 to 2000 cm^{-1}). However, some of the absorption bands of solid products can be assigned to C=O and C–O functional groups [77]. More detailed chemical identification of solid products was performed by GC-MS and is presented later in the subsection 3.4.2.

Figure 6a shows the achieved CB for toluene removal for all tested catalysts in the order as follows: γ-Al_2O_3 (25.5%) < Pd/γ-Al_2O_3 (30.5%) < Pt/γ-Al_2O_3 (36.1%) < TiO_2 (45.7%). The lowest CB was obtained with γ-Al_2O_3, which indicates the greatest formation of undesired products (other than CO_2, CO, and HCOOH), mostly in the form of solid coke deposits. On the other hand, the highest CB was associated with TiO_2 (Figure 6a), accompanied by the highest CO_2 (28.8%), CO (12.7%), and HCOOH (4.1%) selectivities (Figure 6b). In general, all catalysts exhibited similar feature with the highest CO_2 selectivity (from 11.5% to 28.8%), lower CO selectivity (9%–12.7%) and the lowest HCOOH selectivity (1.8%–4.1%). High CO_2 selectivity is generally preferred over CO, as CO_2 is considered a perfect and non-toxic oxidation product of VOC removal [78]. In contrast, CO is the result of incomplete oxidation and, also due to its toxicity, it is desirable to keep its selectivity as low as possible. However, from the perspective of the chemical industry, both CO and HCOOH represent important feedstocks for the production of various fuels and chemicals [79].

3.3 | Regeneration of Coke-Deactivated Catalysts

As mentioned earlier, solid products from the toluene removal gradually accumulated on the surface of the catalysts in the form of coke deposits, and resulted in catalyst fouling and its deactivation. In the next step, a proper catalyst regeneration method can effectively remove them from the surface.

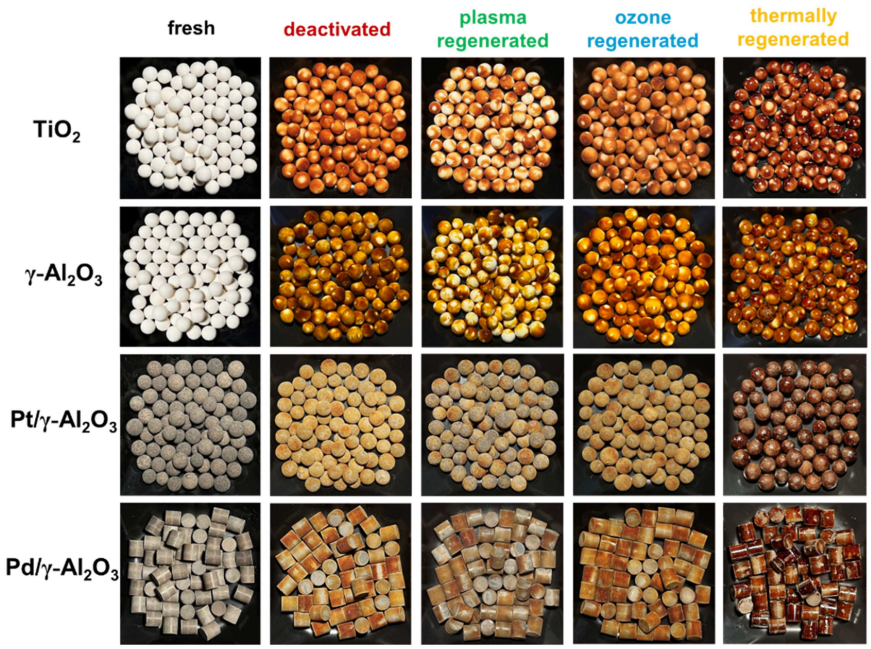

FIGURE 7 | Visual comparison of fresh, deactivated, and regenerated catalysts.

Figure 7 shows photographs of fresh, deactivated (with no regeneration), plasma, ozone, and thermally regenerated catalysts. A significant accumulation of solid coke deposits of brownish color can be observed on the surface of deactivated catalysts compared to their fresh counterparts. Similar deposits after plasma or plasma-catalytic removal of toluene were also observed by other authors [48, 70]. From a visual comparison, it is evident that plasma regeneration achieved the highest reduction in quantity of coke deposits among all tested regeneration methods, although the regeneration was incomplete and non-uniform. Ozone regeneration caused only a subtle lightening of the brownish color of the deposits, while thermal regeneration led to their melting and darkening (Figure 7). Formation of gaseous products of the regeneration along with their qualitative and quantitative characterization is described in the next subsections 3.3.1–3.3.3.

3.3.1 | *Plasma Regeneration*

Figure 8 shows an example of FTIR spectra of gaseous products taken during plasma regeneration. More specifically, comparison of the FTIR spectra obtained with Pt/γ-Al_2O_3 taken at the beginning (i.e., after 6 min) and at the end of the experiment (i.e., after 120 min of discharge operation) is presented. As can be seen, the gaseous products of regeneration were CO_2, CO, HCOOH, and H_2O formed as a result of the oxidation of solid coke deposits. O_3 was also found in the spectra as a typical product of plasma-initiated chemistry in oxygen [80]. In addition, other absorption bands also appeared in the spectra and potentially can be assigned to aromatic C=C and C–H functional groups. Distinct bands between 3000 and 3700 cm^{-1} are also visible, which can be attributed to the absorption of O–H functional group [77].

As can be seen from the comparison of the two spectra, the absorbances (and, thus, concentrations) of all gaseous products changed significantly over time. For this reason, we evaluated detailed time courses of CO_2, CO, HCOOH, and O_3 concentrations during all tested regeneration experiments (Figure 9).

During the plasma regeneration, the concentrations of oxidation products (CO_2, CO, and HCOOH) first increased, after a few minutes reached a maximum, and then gradually decreased (Figure 9a). With exposure to plasma, solid coke deposits began to oxidize, leading to a rapid increase in the concentrations of all oxidation products. Among the tested catalysts, Pt/γ-Al_2O_3 exhibited the highest maximum CO_2 concentration (2730 ppm), while γ-Al_2O_3 showed the lowest maximum (800 ppm). For CO and HCOOH, the highest maxima were obtained with TiO_2 (335 and 350 ppm, respectively), while the lowest maxima with Pd/γ-Al_2O_3 (170 and 50 ppm, respectively). As the plasma regeneration advanced, the catalyst surface was progressively regenerated, leading to a gradual reduction in the quantity of solid coke deposits, which was reflected in the declining production of all oxidation products. The concentration of HCOOH dropped to zero within 50 min of plasma regeneration, while the concentrations of CO_2 and CO remained non-zero throughout the entire regeneration process (Figure 9a). The highest final CO_2 concentration was approx. 1350 ppm for TiO_2, while the highest CO concentration was approx. 90 ppm for Pt/γ-Al_2O_3.

On the contrary to oxidation products, O_3 production under plasma regeneration usually increased over time (Figure 9a). In the beginning of the plasma regeneration, the quantity of solid coke deposits was at maximum, and their oxidation, promoted by reactive oxygen species (·O, ·OH, ...), was the most intense. The consumption of these species was high, leading to low O_3 production. As the plasma regeneration advanced, the quantity of solid coke deposits reduced, and the consumption of reactive oxygen species gradually decreased. Due to their abundance, the O_3 concentration gradually increased, reaching the steady-state value of approx. 8000 ppm (for TiO_2 and Pt/γ-Al_2O_3). However, when comparing the trend of O_3 concentration

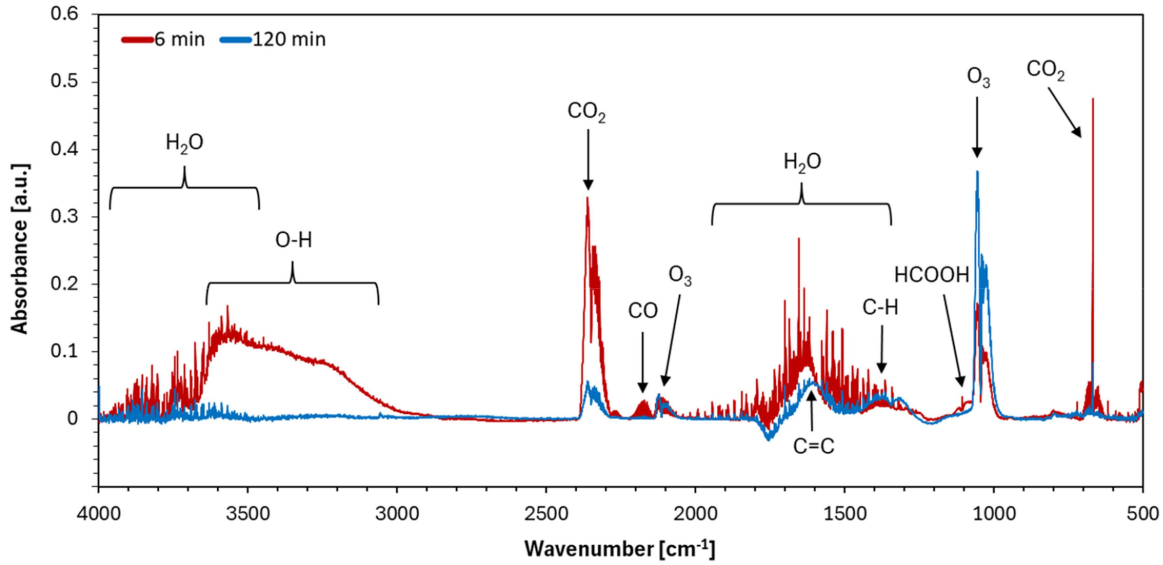

FIGURE 8 | FTIR spectra of products from plasma regeneration of the Pt/γ-Al_2O_3 at different times.

increase for TiO_2 and Pt/γ-Al_2O_3, we observe that the increase is slightly slower for Pt/γ-Al_2O_3. This may be attributed to the moderate activity of Pt catalyst toward O_3 decomposition [81].

For γ-Al_2O_3 (also known as alumina), the steady-state O_3 concentration was lower (approx. 7000 ppm). The γ-Al_2O_3 is commonly used as a support for transition metal oxide catalysts, effective for catalytic O_3 decomposition [82]. However, a few studies investigated the effect of bare γ-Al_2O_3 and showed it may also contribute to the O_3 decomposition [83, 84]. Thomas et al. [85] further showed by experiments and calculations that the O_3 decomposition can readily occur on the γ-Al_2O_3 surface. Several other studies suggest that the O_3 decomposition on γ-Al_2O_3 and metal supported on γ-Al_2O_3 may be due to consumption of surface active sites (SS) via reaction:

$$SS + O_3 \rightarrow SS - O + O_2. \quad (7)$$

In addition, O_3 can be further decomposed at the thus consumed active site to form peroxy species by the following mechanism [84, 86–88]:

$$SS{-}O + O_3 \rightarrow SS - O_2 + O_2. \quad (8)$$

Thomas et al. [85] determined that the surface active sites for the adsorption and decomposition of O_3 on alumina are aluminum ions (Al^{3+}). Based on this, we consider that some degree of O_3 decomposition may potentially occur on the alumina surface and be responsible for a slightly lower steady-state O_3 concentration during plasma regeneration of γ-Al_2O_3.

In contrast to the other catalysts, when Pd/γ-Al_2O_3 was used, the O_3 concentration first increased, but later gradually declined. Kameya and Urano [83] showed that the addition of Pd on MnO_2 catalyst increases the O_3 decomposition, especially under humid gas conditions. A review study by Li et al. [81] reported that in comparison to other noble metal catalysts, Pd exhibits superior O_3 decomposition catalytic activity. Other studies compared the O_3 decomposition activity of Pd and Pt, showing that Pd is more active [89–91]. For these reasons, we speculate that the observed decrease in O_3 concentration may potentially be attributed to this effect. As a result, the final O_3 concentration was approximately 4500 ppm, which is significantly lower than that obtained with other catalysts (Figure 9a).

The fact that the regeneration efficiency is directly related to the amount of reactive oxygen species present in the gas phase was also reported in the studies by Jia et al. [37] and Pinard et al. [22]. The authors investigated the regeneration of coked zeolites using a DBD reactor and, similar to our experiments, observed CO, CO_2, light organic compounds, and carboxylic acids among the regeneration products [37]. Moreover, Di et al. [32] studied the regeneration of similar (Pt, Pd) supported catalysts using a DBD reactor and monitored the time course of CO_2 concentration during the regeneration. They found that even after 130 min of regeneration, the CO_2 concentration did not decrease to zero, indicating the oxidation of solid products on the catalyst surface was still ongoing. A similar conclusion can be drawn from our experiments, where CO_2 and CO concentrations were still significant after 120 min of the catalyst regeneration.

3.3.2 | *Ozone Regeneration*

Figure 9b shows the time courses of the concentrations of major gaseous oxidation products (CO_2, CO, HCOOH) along with O_3 during the ozone regeneration. The catalysts were exposed to a fixed O_3 concentration of approximately 8000 ppm. As the figures show, the O_3 concentration first decreased very sharply, which was accompanied by an increase of oxidation products. This decrease of O_3 can be attributed to its consumption for the oxidation of solid coke deposits. However, the rate of increase and the maximum concentration of oxidation products strictly depended on the catalyst type. While Pt/γ-Al_2O_3 and Pd/γ-Al_2O_3 exhibited a significant increase of oxidation products, for TiO_2 their concentrations remained low. For example, the CO_2 concentration for TiO_2 increased only slightly, while for Pt/γ-Al_2O_3 and Pd/γ-Al_2O_3 it increased rapidly and even reached values close to the values achieved during plasma regeneration with the maxima in a range of 2000–2500 ppm. On the other hand, CO and HCOOH concentrations for all catalysts were

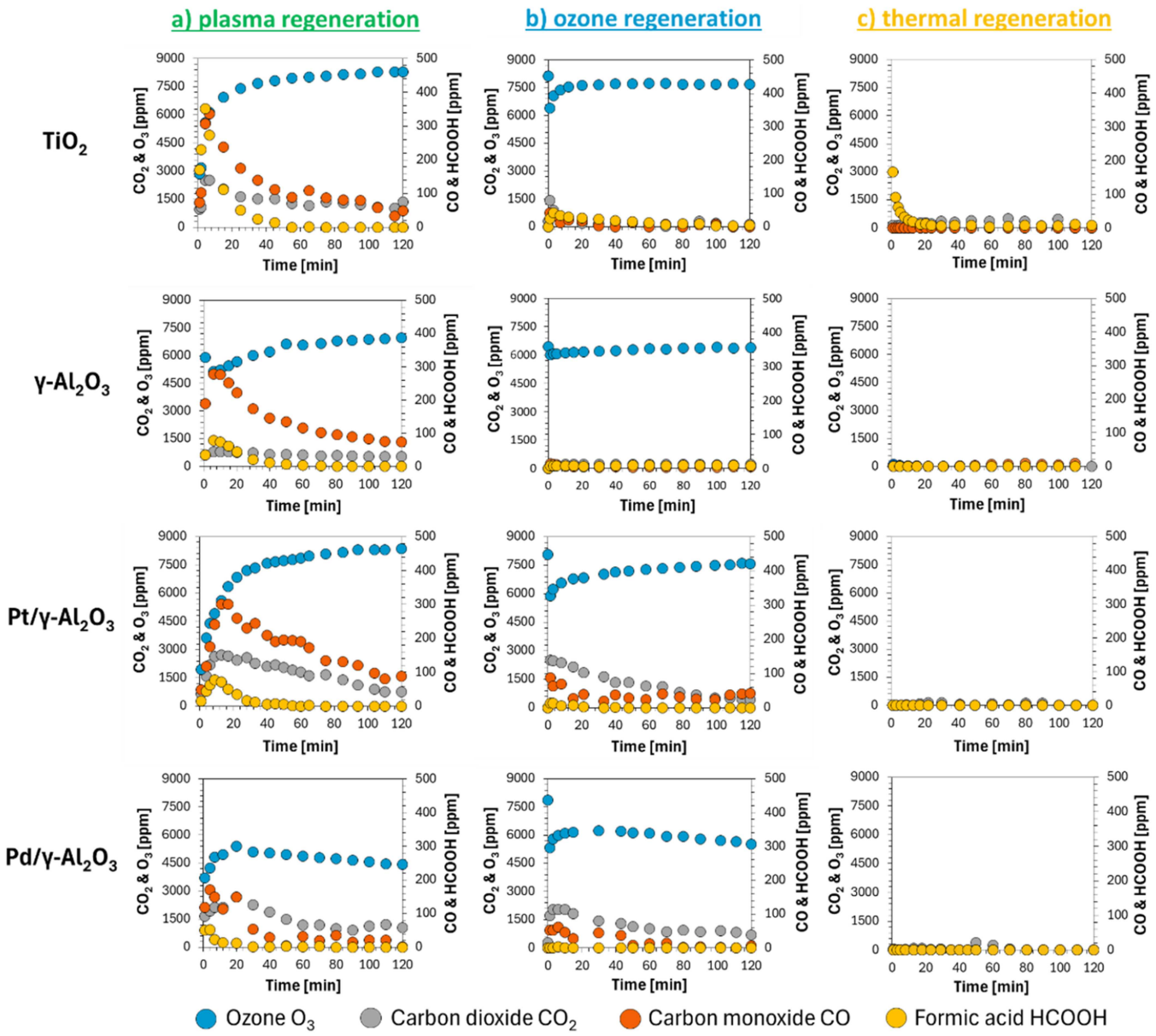

FIGURE 9 | (a–c): Time courses of the concentrations of major gaseous products (CO_2, CO, HCOOH, O_3) for different catalysts during: (a) plasma, (b) ozone, and (c) thermal regeneration.

far from those of the plasma regeneration (CO < 90 ppm, HCOOH < 50 ppm).

After an initial sharp decrease of O_3 concentration, it gradually increased until it reached a concentration of approx. 7600 ppm when TiO_2 and Pt/γ-Al_2O_3 were used. The observed trend is quite reasonable. In the beginning, the amount of solid coke deposits was the biggest. When initially exposed to O_3, their oxidation was the most intense, associated with the greatest O_3 consumption. As time evolved, O_3 consumption gradually decreased, leading to an increase in its concentration at the reactor outlet, which was approximately 400 ppm below the reference value (8000 ppm). This may indicate that a small amount of the produced O_3 was likely still used in the oxidation of coke deposits. Nevertheless, a considerable amount of unoxidized coke deposits remained on the surface of the catalysts. Furthermore, the O_3 concentration increases much slowly for Pt/γ-Al_2O_3 than for TiO_2, which is consistent with the moderate activity of Pt catalyst toward O_3 decomposition, as mentioned in subsection 3.3.1.

The situation with γ-Al_2O_3 and Pd/γ-Al_2O_3 was different. γ-Al_2O_3 showed a relatively small initial decrease in O_3 concentration, followed by a slight increase until it reached a stable value, potentially influenced by O_3 decomposition on the surface, as also discussed earlier in subsection 3.3.1. Compared to other catalysts, γ-Al_2O_3 showed concentrations of oxidation products at their detection limits, indicating negligible oxidation of coke deposits.

In the case of Pd/γ-Al_2O_3, a small increase of O_3 concentration (to approx. 6200 ppm) was followed by a slow decrease (to approx. 5500 ppm). Thus, the O_3 reference concentration was not achieved by the end of the experiment. The explanation could be based on the catalytic decomposition of O_3 over the Pd catalyst [81], as also discussed in the previous subsection 3.3.1.

Moreover, additional measurements with fresh catalysts were conducted to assess their individual activities toward O_3 decomposition. These measurements showed that catalyst activity increases in the following order: $TiO_2 < \gamma\text{-}Al_2O_3 < Pt/\gamma\text{-}Al_2O_3 < Pd/\gamma\text{-}Al_2O_3$, what correlates with the results presented above. Further details are provided in the Supporting Information (Figure S1a–d).

When comparing the results obtained with plasma and ozone regenerations (Figure 9a,b), the production of oxidation products (CO_2, CO, and HCOOH) was lower with ozone regeneration for all catalysts. Along with the visual appearance of catalysts (Figure 7), our results indicate that O_3 has a very limited effect on catalyst regeneration, and its role in the oxidation of solid coke deposits is not crucial. Therefore, the main role in plasma regeneration presumably plays other oxidants, such as reactive oxygen species (e.g., ·O, ·OH, ...). Similar finding was also reported by Jia et al. [37], who stated that the active species responsible for catalyst regeneration are the short-lived oxygenated species and not ozone. Al-Jalal et al. [39] also demonstrated that ·O atoms dominate the process of oxidation of coke. Moreover, Kim et al. [92] performed a similar comparison of oxygen plasma and ozone regeneration of Au/TiO_2 deactivated catalysts by toluene or propylene. They showed that the oxygen plasma treatment exhibited more rapid catalyst regeneration than the O_3 treatment. The fact that the O_3 is not the main oxidizing agent responsible for coke oxidation at low temperature was also reported by Pinard et al. [23].

3.3.3 | *Thermal Regeneration*

Figure 9c shows the time courses of all gaseous oxidation products during the thermal regeneration. For the TiO_2 catalyst, HCOOH was identified as the only oxidation product with a significant concentration increase at the beginning (with a maximum concentration of approx. 165 ppm), followed by its rapid decrease, while the formation of other products was negligible. In contrast, for the $Pt/\gamma\text{-}Al_2O_3$, $Pd/\gamma\text{-}Al_2O_3$, and $\gamma\text{-}Al_2O_3$ catalysts, the concentrations of all oxidation products remained negligible. These findings suggest that the heat produced by the discharge has a minimal or negligible effect on the catalyst regeneration.

When comparing plasma, ozone, and thermal regeneration in terms of energy demand, plasma and ozone regenerations exhibit identical energy demand ($E \approx 1.1$ kWh per one regeneration), as the same HV power supply was used for plasma generation and ozone production. However, ozone regeneration is insufficiently effective in coke removal, despite comparable energy demand. Thermal regeneration requires significantly lower energy input ($E \approx 0.26$ kWh per one regeneration) but is ineffective under the studied conditions. Consequently, plasma regeneration represents the most relevant regeneration approach when both energy use and regeneration efficiency are considered.

3.4 | Advanced Analyses

3.4.1 | *SEM Analysis*

Figure 10a–e presents the SE-SEM micrographs of the fresh, deactivated, plasma, ozone, and thermally regenerated $Pt/\gamma\text{-}Al_2O_3$ catalyst. The SE-SEM micrographs of the fresh (Figure 10a) and deactivated catalyst (Figure 10b) show significant differences in the surface morphological features. The deactivated catalyst had a heavily fouled surface, exhibiting distinct features of solid coke deposits. After ozone regeneration (Figure 10d), there is no evident change in the quantity and shape of the coke deposits. Furthermore, thermal regeneration resulted in melting and hardening of the coke deposits, forming a continuous layer on the catalyst surface (Figure 10e). On the contrary, plasma regeneration led to a reduction of coke deposits (Figure 10c). In Figure 10c, it is visible that some areas of the surface are still occupied by the coke deposit (bottom left) similar to the one in Figure 10b, while the other looks like the fresh catalyst surface (top right) as in Figure 10a. It is clear that the plasma regenerated the catalyst surface non-uniformly and, thus, only partially. In practice, it is quite rare for any catalyst regeneration method to completely remove all foulants from the surface, but regeneration of a significant proportion of the original catalyst surface is desirable [19]. In this sense, the plasma provides an effective alternative to conventional regeneration techniques.

Non-uniform regeneration of the catalyst surface may result from varying discharge characteristics at different locations inside the reactor and, thus, at different locations on the surface of pellets of catalyst. The discharge properties are influenced by many factors, such as the dielectric constant or the shape of the pellets. Materials with a low dielectric constant support formation of surface discharges propagating along the surface of the pellets, whereas materials with a high dielectric constant, promote formation of localized microdischarges between the pellets [51, 93]. Regardless of the pellet material, the electric field is enhanced at the contact points of individual pellets, constraining the discharge and limiting the pellet surface area exposed to the generated plasma and produced reactive species. This effect becomes stronger with increasing dielectric constant of the material [51, 93]. In addition, the electric field enhancement also occurs at the sharp edges of the pellets (especially with cylindrical shape), which further contributes to the spatial localization of the discharge. The nature of the discharge is, thus, closely related not only to the physical properties but also to the shape of the pellets [94]. Therefore, the properties of the pellets significantly affect the propagation and characteristics of the discharge and the production of reactive species in the packed-bed DBD reactors. Varying characteristics of the discharge, along with its localization, may jointly contribute to non-uniform catalyst regeneration. This may be partially eliminated, e.g., by implementing a systematic mixing of the pellets within the reactor. This would help to redistribute the pellets, fostering more uniform conditions for their regeneration and enhancing the overall regeneration efficiency.

3.4.2 | *GC-MS Analysis*

As mentioned earlier, the GC-MS analysis was performed to identify the chemical composition of solid coke deposits accumulated on the surface of the catalysts after both toluene removal and catalyst regeneration experiments. Figure 11a,b presents the measured chromatograms with peaks assigned to the compounds identified in the coke deposits on the deactivated, plasma, ozone, and thermally regenerated $Pt/\gamma\text{-}Al_2O_3$ catalyst. Most of the chromatogram peaks for deactivated, ozone

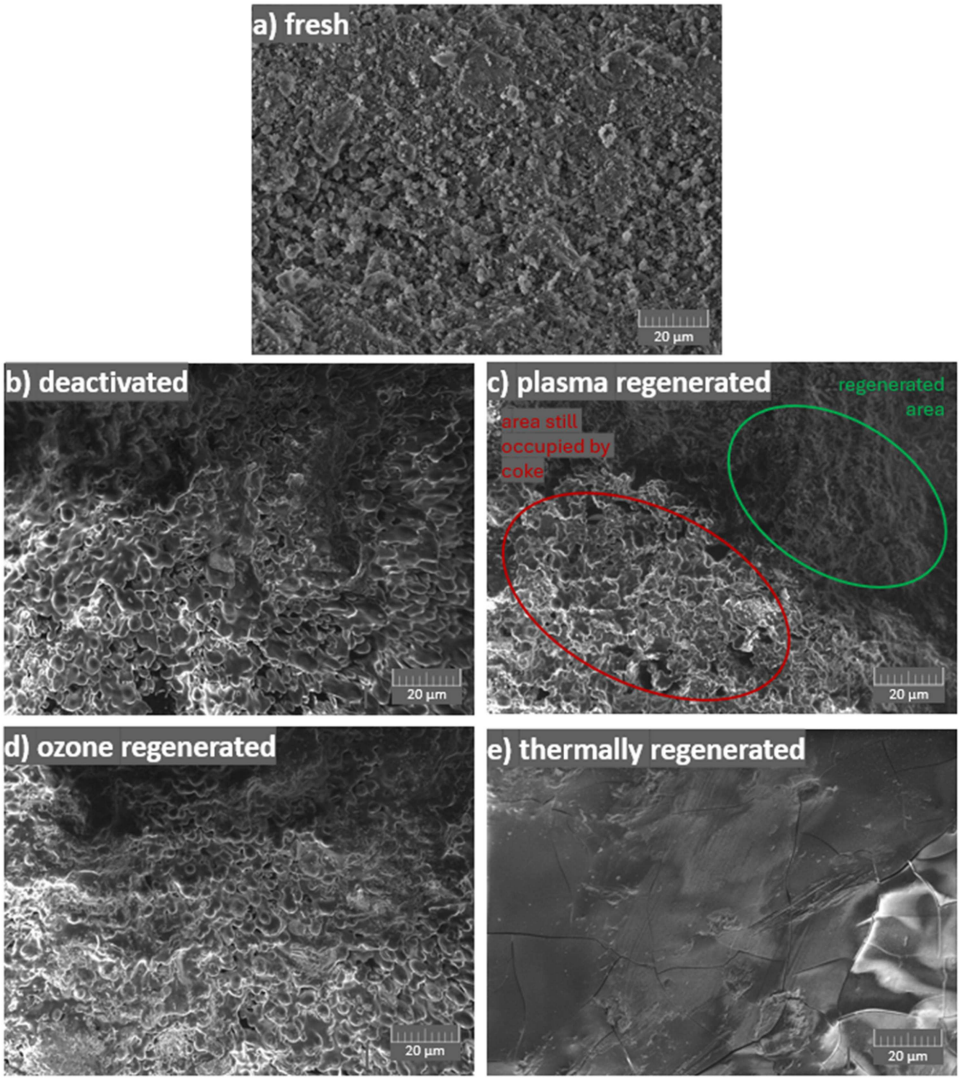

FIGURE 10 | (a–e): SE-SEM micrographs of: (a) fresh, (b) deactivated, (c) plasma, (d) ozone, and (e) thermally regenerated surface of Pt/γ-Al_2O_3.

and thermally regenerated Pt/γ-Al_2O_3 had the same retention time, indicating a comparable chemical composition of coke deposits (Figure 11a). The analysis revealed the presence of compounds from the group of long-chain alkanes and aromatic hydrocarbons. Out of the alkanes, tetradecane and 5-isobutylnonane were recognized. Most of the identified compounds include a functionalized molecule of toluene, benzene or phenol with additional oxygen (e.g., ·OH) or nitrogen-containing (e.g., NO_2) functional groups, e.g., nitro-toluene, nitro-cresol, nitro-phenol, dibenzyl-ether, benzaldehyde, benzoic acid, etc. The products found in the gas phase (CO, CO_2, HCOOH) can be, thus, considered as final products of ring-opening reactions.

It is important to keep in mind that similar molecular structures can give similar mass spectra, and thus some molecules may not necessarily be properly distinguished. This can be, for example, a case when molecules differ only in the position of the functional group on the benzene ring (e.g., 2-nitro-m-cresol, 5-nitro-o-cresol). In the chromatograms, the presented compounds are those with the highest match provided by GC-MS software. In Table 1, the chemical names of the presented compounds are assigned to their structural formulas.

The studies by Liang et al. [70] and Huang et al. [15] analyzed the plasma-catalytic removal of toluene from the air, focusing on detailed analysis of byproducts and toluene decomposition pathways. Among the products, Huang et al. [15] observed CO, CO_2, H_2O, HCOOH, benzene, benzaldehyde, and nitrobenzene. Both papers suggested possible pathways for toluene decomposition. It likely begins with an electron impact reaction that initiates toluene breakdown through H-abstraction from the methyl group. This reaction results in the formation of the benzyl radical that may react with ·O or ·OH to form benzaldehyde with further oxidation to benzoic acid. The aromatic intermediates may further react with ·O, ·OH, ·H, or NO_2, leading to cleavage of the aromatic ring or formation of functionalized molecules, such as nitrobenzene, nitrophenol, cresols, etc. After the ring-opening reactions, small molecular mass compounds, such as CO, HCOOH and acetic acid, are produced. The reactions proceed by a series of oxidation steps mediated mainly by ·O and ·OH, finally leading to the formation of CO_2 and H_2O. Our analysis indicates that the products and intermediates from toluene removal are consistent with those identified by Liang et al. [70] and Huang et al. [15] Therefore, we can conclude that toluene decomposition in our system

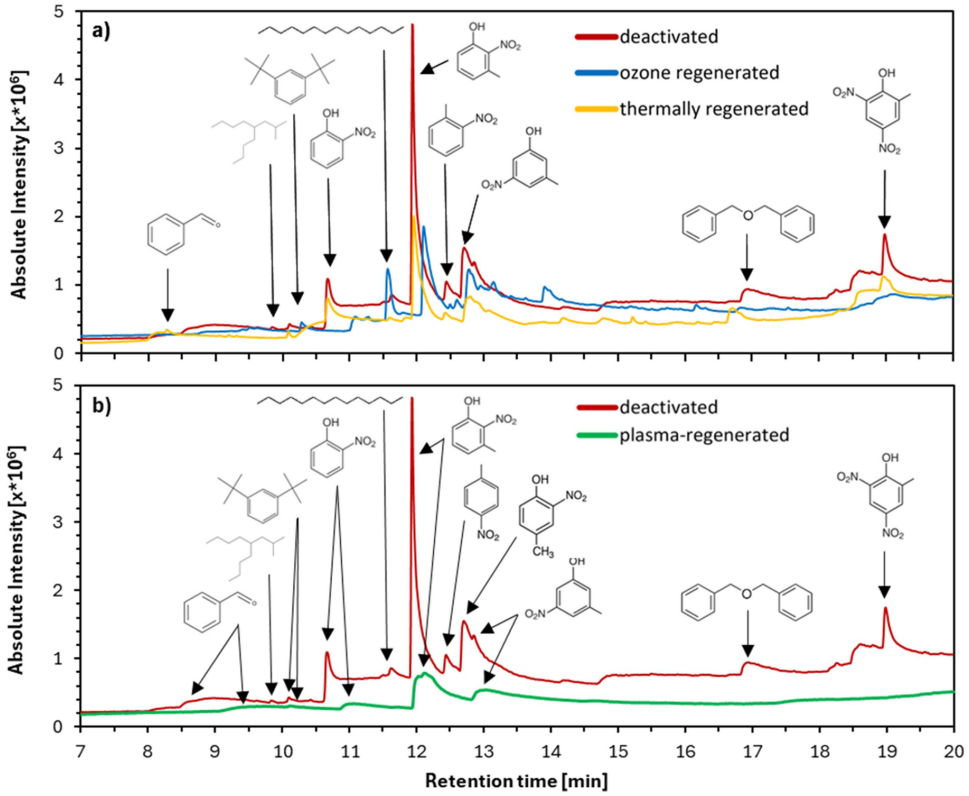

FIGURE 11 | (a, b): GC-MS analysis of coke deposits from deactivated (i.e., without any regeneration), plasma, ozone, and thermally regenerated Pt/γ-Al_2O_3.

TABLE 1 | Structural formulas and chemical names of presented compounds.

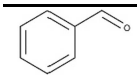	Benzaldehyde	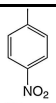	p-Nitro-toluene
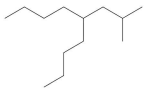	5-Isobutylnonane	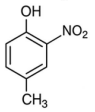	2-Nitro-p-cresol
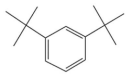	m-Di-tert-butyl-benzene	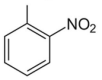	o-Nitro-toluene
	o-Nitro-phenol	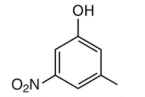	3-Methyl-5-nitro-phenol
	Tetradecane	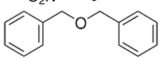	Dibenzyl-ether
	2-Nitro-m-cresol	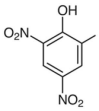	4,6-Dinitro-o-cresol

adheres to the generally proposed reaction pathways for its plasma-catalytic decomposition.

Nevertheless, the chromatogram peaks obtained with the plasma-regenerated catalyst were less numerous and their retention times and intensities were significantly different (Figure 11b). Hence, plasma regeneration significantly reduced the number of compounds that residual coke deposits consisted of and effectively oxidized them into gaseous products. Although a quantitative analysis of products was not performed, lower intensities of chromatogram peaks indicate that the products identified in coke deposits on the surface of the plasma-regenerated catalyst may have a lower concentration than that obtained with ozone and thermally regenerated catalysts.

Finally, the analysis revealed differences in the composition of coke deposits on various catalysts. This is consistent with the results of Rodriguez et al. [95], who reported a different nature of coke formed with each catalyst tested.

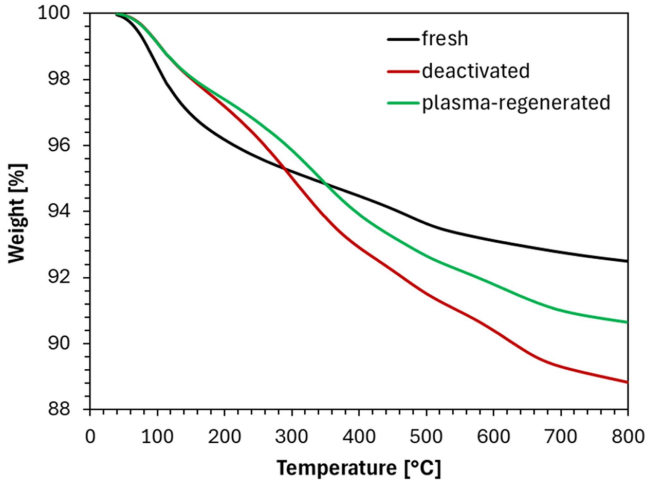

FIGURE 12 | TGA of fresh, deactivated, and plasma-regenerated Pt/γ-Al_2O_3.

3.4.3 | *TGA*

During the TGA, the weight change of the pellets of catalyst was monitored as deposited products gradually desorbed from their surface in response to linear heating. Figure 12 presents the weight change of fresh, deactivated and plasma-regenerated Pt/γ-Al_2O_3 catalyst. Below 100°C, the weight change can be attributed to a release of moisture or other adsorbed impurities from the catalysts, as the thermal regeneration experiment (at 100°C) revealed no major volatile products connected to the coke deposit decomposition indicated by the FTIR. Although the weight change of the fresh catalyst is initially faster (probably due to its greater adsorption capacity and, thus, greater moisture content compared to deactivated and plasma-regenerated catalysts), it slows down at higher temperatures. Up to 140°C, the deactivated and plasma-regenerated catalysts exhibit the same weight change, still probably attributed to the release of moisture. Above 140°C, the weight of the deactivated catalyst ultimately decreases faster than that of the plasma-regenerated one, which we attribute to the gradual release of volatile products associated with the coke deposits. The analysis confirmed that the plasma-regenerated catalyst contained a smaller quantity of volatile coke deposits compared to the deactivated catalyst, which is in correlation with our previous analyses and observations.

4 | Conclusions

This study demonstrated the potential of oxygen NTP for the regeneration of coke-deactivated catalysts. The plasma was generated by a packed-bed DBD reactor operated at atmospheric pressure. Various pellet-shaped materials of distinct catalytic properties (TiO_2, γ-Al_2O_3, Pt/γ-Al_2O_3, and Pd/γ-Al_2O_3) in the pellet form were used in plasma-catalytic VOC removal from the air with toluene as a model target compound. Its removal led to the formation of various products, some of which gradually accumulated on the catalyst surface, creating solid coke deposits that resulted in catalyst deactivation.

Three regeneration techniques (plasma, ozone and thermal) of coke-deactivated catalysts were tested and their efficiency compared. Out of them, the plasma regeneration showed the highest efficiency in oxidizing and removing the coke deposits. The results further indicate that ozone has a very limited effect on catalyst regeneration, and its role in the oxidation of solid coke deposits is not crucial. The effect of heat (100°C) was also found to be negligible. Despite its superior performance, the plasma regeneration was found to be partial and spatially non-uniform, as revealed by SEM and TGA analyses. GC-MS analysis of the coke deposits indicated the presence of long-chain alkanes (e.g., tetradecane) and aromatic hydrocarbons with additional oxygen- or nitrogen-containing functional groups (e.g., nitro-toluene, nitro-cresol, nitro-phenol, benzaldehyde, benzoic acid, etc.). The plasma regeneration significantly reduced the chemical diversity of these compounds in contrast to other regeneration techniques.

Although plasma regeneration represents a promising and environmentally friendly alternative to conventional methods for regenerating coke-deactivated catalysts, further optimization is needed to achieve uniform and advanced regeneration of the catalyst surface. A possible approach to improve uniformity is the implementation of systematic mixing of the catalytic pellets within the reactor. This would help redistribute the pellets during the plasma regeneration, promoting their balanced exposure to plasma-generated reactive species and thereby fostering more uniform conditions for catalyst regeneration and enhancing the overall regeneration efficiency. To comprehensively evaluate the overall effectiveness and feasibility of plasma regeneration, the next research stage should focus on the repetitive use of plasma-regenerated catalysts for plasma-catalytic VOC removal.

Acknowledgments

This work was supported by the Slovak Research and Development Agency Grant APVV-20-0566 and funded by the EU NextGenerationEU through the Recovery and Resilience Plan for Slovakia under the project No. 09I03-03-V04-00092. The authors also thank Dr. Christian Oberste-Beulmann and Prof. Martin Muhler for their help with the GC-MS analysis. We acknowledge Large Research Infrastructure CEPLANT for the provision of its R&D facilities.

Conflicts of Interest

The authors declare no conflicts of interest.

Data Availability Statement

The data that support the findings of this study are available from the corresponding author upon reasonable request.

References

1. H.-H. Kim, A. A. Abdelaziz, Y. Teramoto, et al., "Interim Report of Plasma Catalysis: Footprints in the Past and Blueprints for the Future," *International Journal of Plasma Environmental Science & Technology* 15, no. 1 (2021): e01004, https://doi.org/10.34343/ijpest.2021.15.e01004.

2. M. L. Carreon, "Plasma Catalysis: A Brief Tutorial," *Plasma Research Express* 1, no. 4 (2019): 043001, https://doi.org/10.1088/2516-1067/ab5a30.

3. B. Wang, X. Xu, W. Xu, et al., "The Mechanism of Non-Thermal Plasma Catalysis on Volatile Organic Compounds Removal," *Catalysis Surveys From Asia* 22, no. 2 (2018): 73–94, https://doi.org/10.1007/s10563-018-9241-x.

4. J. Van Durme, J. Dewulf, C. Leys, and H. Van Langenhove, "Combining Non-Thermal Plasma With Heterogeneous Catalysis in Waste Gas Treatment: A Review," *Applied Catalysis, B: Environmental* 78, no. 3–4 (2008): 324–333, https://doi.org/10.1016/j.apcatb.2007.09.035.

5. M. Russo, G. Iervolino, V. Vaiano, and V. Palma, "Non-Thermal Plasma Coupled With Catalyst for the Degradation of Water Pollutants: A Review," *Catalysts* 10, no. 12 (2020): 1438, https://doi.org/10.3390/catal10121438.

6. K. Shang, R. Morent, N. De Geyter, Y. Wang, and Z. Yang, "Plasma Catalytic Degradation of Sulfamethoxazole in Water With Fe/Mn-LDO Catalyst: Performance and Mechanism," *Separation and Purification Technology* 360, no. 3 (2025): 131145, https://doi.org/10.1016/j.seppur.2024.131145.

7. A. George, B. Shen, M. Craven, et al., "A Review of Non-Thermal Plasma Technology: A Novel Solution for CO2 Conversion and Utilization," *Renewable and Sustainable Energy Reviews* 135 (2021): 109702, https://doi.org/10.1016/j.rser.2020.109702.

8. L. Wang, Q. Yin, X. Zhai, and Y. Yi, "Recent Progresses of Plasma-Catalytic CH_4/CO_2 Conversion to Oxygenates: A Short Review," *Current Opinion in Green and Sustainable Chemistry* 51 (2025): 100989, https://doi.org/10.1016/j.cogsc.2024.100989.

9. S. Meng, W. Li, H. Xu, et al., "Non-Thermal Plasma Assisted Catalytic Reforming of Naphtha and Its Model Compounds With Methane at Near Ambient Conditions," *Applied Catalysis, B: Environmental* 297 (2021): 120459, https://doi.org/10.1016/j.apcatb.2021.120459.

10. J. Sun, Z. Qu, Y. Gao, et al., "Plasma Power-to-X (PP2X): Status and Opportunities for Non-Thermal Plasma Technologies," *Journal of Physics D: Applied Physics* 57 (2024): 503002, https://doi.org/10.1088/1361-6463/ad7bc4.

11. L. Baharudin, "A Focused Review of Process Intensification in Methane Dry Reforming to Combat Coke Using Plasma," *Chemical Engineering and Processing - Process Intensification* 194 (2023): 109575, https://doi.org/10.1016/j.cep.2023.109575.

12. Y. S. Mok, E. Jwa, and Y. J. Hyun, "Regeneration of C_4H_{10} Dry Reforming Catalyst by Nonthermal Plasma," *Journal of Energy Chemistry* 22, no. 3 (2013): 394–402, https://doi.org/10.1016/s2095-4956(13)60051-0.

13. R. Cimerman, M. Cíbiková, L. Satrapinskyy, and K. Hensel, "The Effect of Packing Material Properties on Tars Removal by Plasma Catalysis," *Catalysts* 10, no. 12 (2020): 1476, https://doi.org/10.3390/catal10121476.

14. X. Feng, H. Liu, C. He, Z. Shen, and T. Wang, "Synergistic Effects and Mechanism of a Non-Thermal Plasma Catalysis System in Volatile Organic Compound Removal: A Review," *Catalysis Science & Technology* 8, no. 4 (2018): 936–954, https://doi.org/10.1039/C7CY01934C.

15. H. Huang, D. Ye, D. Y. C. Leung, F. Feng, and X. Guan, "Byproducts and Pathways of Toluene Destruction via Plasma-Catalysis," *Journal of Molecular Catalysis A: Chemical* 336, no. 1–2 (2011): 87–93, https://doi.org/10.1016/j.molcata.2011.01.002.

16. J. Van Durme, J. Dewulf, W. Sysmans, C. Leys, and H. Van Langenhove, "Abatement and Degradation Pathways of Toluene in Indoor Air by Positive Corona Discharge," *Chemosphere* 68, no. 10 (2007): 1821–1829, https://doi.org/10.1016/j.chemosphere.2007.03.053.

17. C. Bartholomew, *"Catalyst Deactivation and Regeneration," In:* Kirk-Othmer Encyclopedia of Chemical Technology (John Wiley and Sons, 2003), 255–322.

18. M. Argyle and C. Bartholomew, "Heterogeneous Catalyst Deactivation and Regeneration: A Review," *Catalysts* 5, no. 1 (2015): 145–269, https://doi.org/10.3390/catal5010145.

19. D. L. Trimm, "The Regeneration or Disposal of Deactivated Heterogeneous Catalysts," *Applied Catalysis, A: General* 212, no. 1–2 (2001): 153–160, https://doi.org/10.1016/S0926-860X(00)00852-8.

20. B. Chen, L. Wu, B. Wu, et al., "Catalytic Materials for Low Concentration VOCs Removal Through 'Storage - Regeneration' Cycling," *ChemCatChem* 11, no. 16 (2019): 3646–3661, https://doi.org/10.1002/cctc.20190058.

21. M. Mozetič, A. Vesel, G. Primc, and R. Zaplotnik, *"Introduction to Plasma and Plasma Diagnostics," In: Non-Thermal* Plasma Technology for Polymeric Materials (Elsevier, 2019), 23–65, https://doi.org/10.1016/b978-0-12-813152-7.00002-0.

22. L. Pinard, N. Ayoub, and C. Batiot-Dupeyrat, "Regeneration of a Coked Zeolite via Nonthermal Plasma Process: A Parametric Study," *Plasma Chemistry and Plasma Processing* 39 (2019): 929–936, https://doi.org/10.1007/s11090-019-09972-x.

23. L. Pinard and C. Batiot-Dupeyrat, "Non-Thermal Plasma for Catalyst Regeneration: A Review," *Catalysis Today* 426 (2024): 114372, https://doi.org/10.1016/j.cattod.2023.114372.

24. S. Shao, Z. Ye, J. Sun, et al., "A Review on the Application of Non-Thermal Plasma (NTP) in the Conversion of Biomass: Catalyst Preparation, Thermal Utilization and Catalyst Regeneration," *Fuel* 330 (2022): 125420, https://doi.org/10.1016/j.fuel.2022.125420.

25. M. Kim, J. Jeoung, J. Kim, and K.-S. Ha, "Regeneration of Deactivated H-ZSM-5 for Aromatization by Dielectric Barrier Discharge Plasma," *Applied Catalysis, A: General* 575 (2019): 214–222, https://doi.org/10.1016/j.apcata.2019.02.027.

26. Y. Fan, G. Hou, Y. Xiong, C. Chen, and W. Zhao, "Co-Upgrading of Biomass and Plastic Volatiles *via* Metal-Modified HZSM-5 Coupled With NTP: Deterioration and *in Situ* Recovery of the Catalyst," *Catalysis Science & Technology* 10 (2020): 7965–7983, https://doi.org/10.1039/D0CY01473G.

27. H. Chen, Y. Mu, S. Xu, S. Xu, C. Hardacre, and X. Fan, "Recent Advances in Non-Thermal Plasma (NTP) Catalysis Towards C1 Chemistry," *Chinese Journal of Chemical Engineering* 28, no. 8 (2020): 2010–2021, https://doi.org/10.1016/j.cjche.2020.05.027.

28. P. Mehta, P. Barboun, D. B. Go, J. C. Hicks, and W. F. Schneider, "Catalysis Enabled by Plasma Activation of Strong Chemical Bonds: A Review," *ACS Energy Letters* 4, no. 5 (2019): 1115–1133, https://doi.org/10.1021/acsenergylett.9b00263.

29. D. H. Lee, Y.-H. Song, K.-T. Kim, S. Jo, and H. Kang, "Current State and Perspectives of Plasma Applications for Catalyst Regeneration," *Catalysis Today* 337 (2019): 15–27, https://doi.org/10.1016/j.cattod.2019.04.071.

30. M. M. Hossain, Y. S. Mok, D. B. Nguyen, R. Ahmed, S. S. Saud, and I. Heo, "Effective Removal of Toluene at Near Room Temperature Using Cyclic Adsorption-Oxidation Operation in Alternative Fixed-Bed Plasma-Catalytic Reactor," *Chemical Engineering Research and Design* 164 (2020): 299–310, https://doi.org/10.1016/j.cherd.2020.10.006.

31. D.-Z. Zhao, X.-S. Li, C. Shi, H.-Y. Fan, and A.-M. Zhu, "Low-Concentration Formaldehyde Removal From Air Using a Cycled Storage–Discharge (CSD) Plasma Catalytic Process," *Chemical Engineering Science* 66, no. 17 (2011): 3922–3929, https://doi.org/10.1016/j.ces.2011.05.019.

32. S. Di, J. Xu, S. Yao, et al., "Room-Temperature Degradation of O-Xylene in Simulated Air Using an Online-Regenerable Plasma-Catalysis Reactor With Low Amounts of Nanosized Noble Metals on Co_3O_4," *Plasma Science and Technology* 25, no. 10 (2023): 104003, https://doi.org/10.1088/2058-6272/acde32.

33. S. Kaliya Perumal Veerapandian, J. M. Giraudon, N. De Geyter, et al., "Regeneration of Hopcalite Used for the Adsorption Plasma Catalytic Removal of Toluene by Non-Thermal Plasma," *Journal of Hazardous Materials* 402 (2021): 123877, https://doi.org/10.1016/j.jhazmat.2020.123877.

34. Y. S. Mok and D. H. Kim, "Treatment of Toluene by Using Adsorption and Nonthermal Plasma Oxidation Process," *Current Applied Physics* 11, no. 5 (2011): S58–S62, https://doi.org/10.1016/j.cap.2011.05.023.

35. W. Wang, T. Zhu, and X. Fan, *"Removal of Gas Phase Low-concentration Toluene by Intermittent Use of Adsorption and Non-Thermal Plasma Regeneration," 21st International Symposium on Plasma Chemistry (ISPC 21)* (Cairns Convention Centre, 2013).

36. T. Kuroki, T. Fujioka, R. Kawabata, M. Okubo, and T. Yamamoto, "Regeneration of Honeycomb Zeolite by Nonthermal Plasma Desorption of Toluene," *IEEE Transactions on Industry Applications* 45, no. 1 (2009): 10–15, https://doi.org/10.1109/tia.2008.2009476.

37. L. Y. Jia, A. Farouha, L. Pinard, et al., "New Routes for Complete Regeneration of Coked Zeolite," *Applied Catalysis, B: Environmental* 219 (2017): 82–91, https://doi.org/10.1016/j.apcatb.2017.07.040.

38. H. Srour, E. Devers, A. Mekki-Berrada, et al., "Regeneration of an Aged Hydrodesulfurization Catalyst: Conventional Thermal vs Non-Thermal Plasma Technology," *Fuel* 306 (2021): 121674, https://doi.org/10.1016/j.fuel.2021.121674.

39. A. M. Al-Jalal and M. A. Khan, "Optical Emission and Raman Spectroscopy Studies of Reactivity of Low-Pressure Glow Discharges in Ar-O_2 and He-O_2 Gas Mixtures With Coked Catalysts," *Plasma Chemistry and Plasma Processing* 30 (2010): 173–182, https://doi.org/10.1007/s11090-009-9201-3.

40. M. Trueba and S. P. Trasatti, "γ-Alumina as a Support for Catalysts: A Review of Fundamental Aspects," *European Journal of Inorganic Chemistry* 2005, no. 17 (2005): 3393–3403, https://doi.org/10.1002/ejic.200500348.

41. H. Pines and W. O. Haag, "Alumina: Catalyst and Support. I. Alumina, Its Intrinsic Acidity and Catalytic Activity," *Journal of the American Chemical Society* 82, no. 10 (1960): 2471–2483, https://doi.org/10.1021/ja01495a021.

42. J. Fisher and T. A. Egerton, *"Titanium Compounds, Inorganic," In: Kirk-Othmer Encyclopedia of Chemical Technology* (John Wiley and Sons, 2001), https://doi.org/10.1002/0471238961.0914151805070518.a01.pub2.

43. A. S. Ivanova, E. M. Slavinskaya, R. V. Gulyaev, et al., "Metal–Support Interactions in Pt/Al2O3 and Pd/Al2O3 Catalysts for CO Oxidation," *Applied Catalysis, B: Environmental* 97, no. 1–2 (2010): 57–71, https://doi.org/10.1016/j.apcatb.2010.03.024.

44. C. Morterra and G. Magnacca, "A Case Study: Surface Chemistry and Surface Structure of Catalytic Aluminas, as Studied by Vibrational Spectroscopy of Adsorbed Species," *Catalysis Today* 27, no. 3–4 (1996): 497–532, https://doi.org/10.1016/0920-5861(95)00163-8.

45. R. Cimerman, D. Račková, and K. Hensel, "Tars Removal by Non-Thermal Plasma and Plasma Catalysis," *Journal of Physics D: Applied Physics* 51, no. 27 (2018): 274003, https://doi.org/10.1088/1361-6463/aac762.

46. R. Brandenburg, "Dielectric Barrier Discharges: Progress on Plasma Sources and on the Understanding of Regimes and Single Filaments," *Plasma Sources Science and Technology* 26, no. 5 (2017): 053001, https://doi.org/10.1088/1361-6595/aa6426.

47. R. Wang, Y. Yang, S. Chen, H. Jiang, and P. Martin, "Power Calculation of Pulse Power-Driven DBD Plasma," *IEEE Transactions on Plasma Science* 49, no. 7 (2021): 2210–2216, https://doi.org/10.1109/TPS.2021.3084601.

48. C. Oberste-Beulmann, T. Oppotsch, and M. Muhler, "The Effect of Toluene Trace Admixtures on the Plasma-Assisted Oxygen Trace Removal From Hydrogen-Rich Gas Mixtures in a Surface Dielectric Barrier Discharge Reactor," *Plasma Processes and Polymers* 20, no. 10 (2023): e2300084, https://doi.org/10.1002/ppap.202300084.

49. Z. Falkenstein and J. J. Coogan, "Microdischarge Behaviour in the Silent Discharge of Nitrogen–Oxygen and Water–Air Mixtures," *Journal of Physics D: Applied Physics* 30, no. 5 (1997): 817–825, https://doi.org/10.1088/0022-3727/30/5/015.

50. K. Van Laer and A. Bogaerts, "How Bead Size and Dielectric Constant Affect the Plasma Behaviour in a Packed Bed Plasma Reactor: A Modelling Study," *Plasma Sources Science and Technology* 26, no. 8 (2017): 085007, https://doi.org/10.1088/1361-6595/aa7c59.

51. W. Wang, H.-H. Kim, K. Van Laer, and A. Bogaerts, "Streamer Propagation in a Packed Bed Plasma Reactor for Plasma Catalysis Applications," *Chemical Engineering Journal* 334 (2018): 2467–2479, https://doi.org/10.1016/J.CEJ.2017.1.139.

52. Q.-Z. Zhang and A. Bogaerts, "Propagation of a Plasma Streamer in Catalyst Pores," *Plasma Sources Science and Technology* 27, no. 3 (2018): 035009, https://doi.org/10.1088/1361-6595/aab47a.

53. J. Kruszelnicki, K. W. Engeling, J. E. Foster, and M. J. Kushner, "Interactions Between Atmospheric Pressure Plasmas and Metallic Catalyst Particles in Packed Bed Reactors," *Journal of Physics D: Applied Physics* 54, no. 10 (2020): 104001, https://doi.org/10.1088/1361-6463/abcc92.

54. A. Wypych, I. Bobowska, M. Tracz, et al., "Dielectric Properties and Characterisation of Titanium Dioxide Obtained by Different Chemistry Methods," *Journal of Nanomaterials* 2014, no. 1 (2014): 124814, https://doi.org/10.1155/2014/124814.

55. H.-H. Kim, Y. Teramoto, N. Negishi, and A. Ogata, "A Multidisciplinary Approach to Understand the Interactions of Nonthermal Plasma and Catalyst: A Review," *Catalysis Today* 256, no. 1 (2015): 13–22, https://doi.org/10.1016/j.cattod.2015.04.009.

56. K. W. Engeling, J. Kruszelnicki, M. J. Kushner, and J. E. Foster, "Time-Resolved Evolution of Micro-Discharges, Surface Ionization Waves and Plasma Propagation in a Two-Dimensional Packed Bed Reactor," *Plasma Sources Science and Technology* 27, no. 8 (2018): 085002, https://doi.org/10.1088/1361-6595/aad2c5.

57. R. Burch and P. K. Loader, "Investigation of Pt/Al_2O_3 and Pd/Al_2O_3 Catalysts for the Combustion of Methane at Low Concentrations," *Applied Catalysis, B: Environmental* 5, no. 1–2 (1994): 149–164, https://doi.org/10.1016/0926-3373(94)00037-9.

58. D. Mei, X. Zhu, C. Wu, B. Ashford, P. T. Williams, and X. Tu, "Plasma-Photocatalytic Conversion of CO_2 at Low Temperatures: Understanding the Synergistic Effect of Plasma-Catalysis," *Applied Catalysis, B: Environmental* 182 (2016): 525–532, https://doi.org/10.1016/j.apcatb.2015.09.052.

59. E. C. Neyts, "Plasma-Surface Interactions in Plasma Catalysis," *Plasma Chemistry and Plasma Processing* 36 (2016): 185–212, https://doi.org/10.1007/s11090-015-9662-5.

60. H.-H. Kim, S. M. Oh, A. Ogata, and S. Futamura, "Decomposition of Gas-Phase Benzene Using Plasma-Driven Catalyst (PDC) Reactor Packed With Ag/TiO2 Catalyst," *Applied Catalysis, B: Environmental* 56 (2005): 213–220, https://doi.org/10.1016/J.APCATB.2004.09.008.

61. T. Butterworth and R. W. K. Allen, "Plasma-Catalyst Interaction Studied in a Single Pellet DBD Reactor: Dielectric Constant Effect on Plasma Dynamics," *Plasma Sources Science and Technology* 26 (2017): 065008, https://doi.org/10.1088/1361-6595/aa6c35.

62. G. Iervolino, T. Russo, and V. Vaiano, "Catalytic Non-Thermal Plasma Reactor Operating at Low Applied Voltage for the Removal of Toluene in Air," *Environmental Technology & Innovation* 34 (2024): 103550, https://doi.org/10.1016/j.eti.2024.103550.

63. A. M. Vandenbroucke, R. Morent, N. D. Geyter, and C. Leys, "Decomposition of Toluene With Plasma-Catalysis: A Review," *Journal of Advanced Oxidation Technologies* 15 (2012): 232–241, https://doi.org/10.1515/jaots-2012-0201.

64. G. Xiao, W. Xu, R. Wu, et al., "Non-Thermal Plasmas for VOCs Abatement," *Plasma Chemistry and Plasma Processing* 34 (2014): 1033–1065, https://doi.org/10.1007/s11090-014-9562-0.

65. S. Veerapandian, C. Leys, N. De Geyter, and R. Morent, "Abatement of VOCs Using Packed Bed Non-Thermal Plasma Reactors: A Review," *Catalysts* 7 (2017): 113, https://doi.org/10.3390/catal7040113.

66. A. M. Harling, H.-H. Kim, S. Futamura, and J. C. Whitehead, "Temperature Dependence of Plasma-Catalysis Using a Nonthermal,

Atmospheric Pressure Packed Bed; the Destruction of Benzene and Toluene," *Journal of Physical Chemistry C* 111 (2007): 5090–5095, https://doi.org/10.1021/jp067821w.

67. H.-H. Kim, A. Ogata, and S. Futamura, "Effect of Different Catalysts on the Decomposition of VOCs Using Flow-Type Plasma-Driven Catalysis," *IEEE Transactions on Plasma Science* 34 (2006): 984–995, https://doi.org/10.1109/TPS.2006.875728.

68. F. Holzer, "Combination of Non-Thermal Plasma and Heterogeneous Catalysis for Oxidation of Volatile Organic Compounds. Part 1. Applied Catalysis B: Environmental," *Applied Catalysis, B: Environmental* 38 (2002): 163–181, https://doi.org/10.1016/S0926-3373(02)00040-1.

69. Y.-H. Song, S.-J. Kim, K.-I. Choi, and T. Yamamoto, "Effects of Adsorption and Temperature on a Nonthermal Plasma Process for Removing VOCs," *Journal of Electrostatics* 55 (2002): 189–201, https://doi.org/10.1016/S0304-3886(01)00197-8.

70. W.-J. Liang, L. Ma, H. Liu, and J. Li, "Toluene Degradation by Non-Thermal Plasma Combined With a Ferroelectric Catalyst," *Chemosphere* 92 (2013): 1390–1395, https://doi.org/10.1016/j.chemosphere.2013.05.042.

71. W. Liang, A. Wang, L. Ma, and J. Li, "Combination of Spontaneous Polarization Plasma and Photocatalyst for Toluene Oxidation," *Journal of Electrostatics* 75 (2015): 27–34, https://doi.org/10.1016/j.elstat.2015.02.007.

72. B. Wang, S. Yao, Y. Peng, and Y. Xu, "Toluene Removal over TiO2-BaTiO3 Catalysts in an Atmospheric Dielectric Barrier Discharge," *Journal of Environmental Chemical Engineering* 6 (2018): 3819–3826, https://doi.org/10.1016/j.jece.2018.06.006.

73. T. Zhu, J. Li, W. Liang, and Y. Jin, "Synergistic Effect of Catalyst for Oxidation Removal of Toluene"," *Journal of Hazardous Materials* 165 (2009): 1258–1260, https://doi.org/10.1016/j.jhazmat.2008.10.085.

74. M. Kang, B. J. Kim, S. M. Cho, et al., "Decomposition of Toluene Using an Atmospheric Pressure Plasma/TiO2 Catalytic System," *Journal of Molecular Catalysis A: Chemical* 180 (2002): 125–132, https://doi.org/10.1016/S1381-1169(01)00417-4.

75. C. L. Chang and T. S. Lin, "Decomposition of Toluene and Acetone in Packed Dielectric Barrier Discharge Reactors," *Plasma Chemistry and Plasma Processing* 25 (2005): 227–243, https://doi.org/10.1007/s11090-004-3034-x.

76. W. Zhou, Z. Guan, M. Zhao, and J. Li, "Characteristics and Mechanism of Toluene Removal From Gas by Novelty Array Double Dielectric Barrier Discharge Combined With TiO2/Al2O3 Catalyst," *Chemosphere* 226 (2019): 766–773, https://doi.org/10.1016/j.chemosphere.2019.04.005.

77. G. Socrates, *Infrared and Raman Characteristic Group Frequencies - Tables and Charts* (John Wiley & Sons Ltd, 2001).

78. W. Liu, Z. Zhang, K. Yuan, et al., "Catalytic Oxidation Degradation of Volatile Organic Compounds (VOCs) – A Review," *Reviews in Inorganic Chemistry* 44 (2023): 209–229, https://doi.org/10.1515/revic-2023-0015.

79. R. Snoeckx and A. Bogaerts, "Plasma Technology – a Novel Solution for CO2 Conversion?," *Chemical Society Reviews* 46 (2017): 5805–5863, https://doi.org/10.1039/C6CS00066E.

80. B. Eliasson and U. Kogelschatz, "Nonequilibrium Volume Plasma Chemical Processing," *IEEE Transactions on Plasma Science* 19 (1991): 1063–1077.

81. X. Li, J. Ma, and H. He, "Recent Advances in Catalytic Decomposition of Ozone," *Journal of Environmental Sciences* 94 (2020): 14–31, https://doi.org/10.1016/j.jes.2020.03.058.

82. J. Lu, S. Wang, K. Zhao, et al., "Study on Catalytic Performance of Supported Transition Metal Oxide Catalyst for Ozone Decomposition," *Journal of Fuel Chemistry and Technology* 49 (2021): 1014–1022, https://doi.org/10.1016/S1872-5813(21)60044-0.

83. T. Kameya and K. Urano, "Catalytic Decomposition of Ozone Gas by a Pd Impregnated MnO2 Catalyst," *Journal of Environmental Engineering* 128 (2002): 286–292, https://doi.org/10.1061/(ASCE)0733-9372(2002)128:3(286).

84. R. C. Sullivan, T. Thornberry, and J. P. D. Abbatt, "Ozone Decomposition Kinetics on Alumina: Effects of Ozone Partial Pressure, Relative Humidity and Repeated Oxidation Cycles," *Atmospheric Chemistry and Physics* 4 (2004): 1301–1310.

85. K. Thomas, P. E. Hoggan, L. Mariey, J. Lamotte, and J. C. Lavalley, "Experimental and Theoretical Study of Ozone Adsorption on Alumina," *Catalysis Letters* 46 (1997): 77–82, https://doi.org/10.1023/A:1019017123596.

86. W. Xue, B. Gu, Y. Jiang, et al., "Pd-Enhanced Carbon Catalyst for Efficient Ozone Removal via Tuning Carbon Electronic Properties," *Carbon* 238 (2025): 120162, https://doi.org/10.1016/j.carbon.2025.120162.

87. B. Dhandapani and S. T. Oyama, "Gas Phase Ozone Decomposition Catalysts," *Applied Catalysis, B: Environmental* no 11 (1997): 129–166, https://doi.org/10.1016/S0926-3373(96)00044-6.

88. C. Cheng, Y. Zou, J. Li, et al., "Adsorption and Reaction Mechanisms of Direct Palladium Synthesis by ALD Using Pd(hfac)2 and Ozone on Si (100) Surface," *Processes* no 9 (2021): 2246, https://doi.org/10.3390/pr9122246.

89. R. M. Heck, R. J. Farrauto, and H. C. Lee, "Commercial Development and Experience With Catalytic Ozone Abatement in Jet Aircraft," *Catalysis Today* 13 (1992): 43–58, https://doi.org/10.1016/0920-5861(92)80186-Q.

90. C. L. Chang and L. Tser-Sheng lin, "Pt/Rh and Pd/Rh Catalysts Used for Ozone Decomposition and Simultaneous Elimination of Ozone and Carbon Monoxide," *Reaction Kinetics and Catalysis Letters* 86 (2005): 91–98.

91. M. C. Wu and N. A. Kelly, "Clean-Air Catalyst System for on-Road Applications: I. Evaluation of Potential Catalysts," *Applied Catalysis, B: Environmental* 18 (1998): 79–91, https://doi.org/10.1016/S0926-3373(98)00027-7.

92. H.-H. Kim, S. Tsubota, M. Daté, A. Ogata, and S. Futamura, "Catalyst Regeneration and Activity Enhancement of Au/TiO2 by Atmospheric Pressure Nonthermal Plasma," *Applied Catalysis, A: General* 329 (2007): 93–98, https://doi.org/10.1016/j.apcata.2007.06.029.

93. K. Van Laer and A. Bogaerts, "Influence of Gap Size and Dielectric Constant of the Packing Material on the Plasma Behaviour in a Packed Bed DBD Reactor: A Fluid Modelling Study," *Plasma Processes and Polymers* 14 (2017): 1600129, https://doi.org/10.1002/PPAP.201600129.

94. A. Bogaerts, X. Tu, J. C. Whitehead, et al., "The 2020 Plasma Catalysis Roadmap," *Journal of Physics D: Applied Physics* 53 (2020): 443001, https://doi.org/10.1088/1361-6463/ab9048.

95. A. C. Rodriguez, M. E. Sad, H. Cruchade, L. Pinard, and C. L. Padró, "Study of Catalyst Deactivation During 1,3-Butanediol Dehydration to Produce Butadiene," *Microporous and Mesoporous Materials* 320 (2021): 111066, https://doi.org/10.1016/j.micromeso.2021.111066.

Supporting Information

Additional supporting information can be found online in the Supporting Information section.
Supporting File: ppap70166-sup-0001-Supplementary_material.docx.